Ocean dynamics
Volume 57, Numbers 4-5 / octobre 2007
http://dx.doi.org/10.1007/s10236-007-0115-4

High-resolution atmospheric forcing for regional oceanic model: the Iroise Sea

Héloïse Muller[1,] *, Franck Dumas[2], Bruno Blanke[1] and Vincent Mariette[3]

[1]Laboratoire de Physique des Océans (LPO)/University of Western Brittany, UMR 6523 CNRS/IFREMER/UBO, UFR Sciences et Techniques, 6 Avenue Le Gorgeu, BP 809, 29285 Brest Cedex, France
[2]IFREMER/DYNECO-PHYSED, BP70, 29280 Plouzane France Cedex, France
[3]ACTIMAR, 24 Quai de la Douane, 29200 Brest Cedex, France

*: Corresponding author : Héloïse Muller, Email: heloise.muller@ifremer.fr

Abstract:

This study was aimed at modeling, as realistically as possible, the dynamics and thermodynamics of the Iroise Sea by using the Model for Applications at Regional Scale (MARS), a regional ocean 3D model. The horizontal resolution of the configuration in use is 2 km with 30 vertical levels. The 3D model of the Iroise Sea is embedded in a larger model providing open boundary conditions. As regards the atmospheric forcing, the originality of this study is to force the regional ocean model with the high-resolution (6 km) regional meteorological model, Weather Research and Forecasting (WRF). In addition, as the air surface temperature is highly sensitive to the sea surface temperature (SST), this regional meteorological model is improved by taking into account a regional climatologic SST to compute meteorological parameters. By allowing a better coherence between the SST and the temperature of the atmospheric boundary layer while giving a more realistic representation of heat fluxes exchanged at the air/sea interface, this forcing constitutes a noticeable improvement of the Iroise Sea modeling. The different sensitivity tests discussed here pinpoint the importance of entering, in WRF, SST data of sufficiently high quality before the computation of meteorological forcing when the aim is a study of dynamics and thermodynamics far away from the coast. On the other hand, when the target is the reproduction of coastal small-scale features in Iroise Sea modeling, the resolution of the meteorological forcing and the quality of SST are both paramount. The simulation of reference was carried out throughout the Summer and Autumn of year 2005 to allow comparisons with a campaign of surface current measurements by high-frequency radars conducted at the same period.

Keywords: Iroise Sea - MARS - WRF - High-frequency radar data

Abstract

This study was aimed at modelling, as realistically as possible, the dynamics and thermodynamics of the Iroise Sea by using MARS, a regional ocean 3D model. The horizontal resolution of the configuration in use is 2 km with 30 vertical levels. The 3D model of the Iroise Sea is embedded in a larger model providing open boundary conditions. As regards the atmospheric forcing, the originality of this study is to force the regional ocean model with the high-resolution (6 km) regional meteorological model, WRF. In addition, as the air surface temperature is highly sensitive to the sea surface temperature, this regional meteorological model is improved by taking into account a regional climatologic sea surface temperature in order to compute meteorological parameters.

By allowing a better coherence between the sea surface temperature and the temperature of the atmospheric boundary layer while giving a more realistic representation of heat fluxes exchanged at the air/sea interface, this forcing constitutes a noticeable improvement of the Iroise Sea modelling. The different sensitivity tests discussed here pinpoint the importance of entering, in WRF, sea surface temperature data of sufficiently high quality prior to the computation of meteorological forcing when the aim is a study of dynamics and thermodynamics far away from the coast. On the other hand, when the target is the reproduction of coastal small-scale features in Iroise Sea modelling, the resolution of the meteorological forcing and the quality of sea surface temperature are both paramount. The simulation of reference was carried out throughout the Summer and Autumn of year 2005 in order to allow comparisons with a campaign of surface current measurements by High Frequency (HF) radars conducted at the same period.

Keywords: Iroise Sea, MARS, WRF, High frequency radar data

1 Introduction

The Iroise Sea is located at the western end of Brittany (France). It is a shallow area with a mean depth of 110 m. With regard to the hydrodynamics, the tidal wave is semi diurnal and propagates northwards at the extreme end of Brittany. The interaction with the coastline and bathymetry causes strong currents along the North coast (1.55 m/s), around the islands of Sein and Ushant and in constricted areas. Though they can reach up to 4.11 m/s at spring tides in certain fairways (Le Duff, Hily 1999), locally they are rather weak in the bays, between the islands and along the South coast (0.51 m/s). The circulation, whose local intensity varies from one region to another one, is also constrained by surface wind stress-generated currents and waves.

Getting a deep insight into the Lagrangian circulation in the Iroise Sea is essential because this area of intense maritime traffic is permanently at risk of accidental pollution; in addition, its frontal regions are also the sites of intense biological activity. But, a prerequisite to any accurate diagnostic of Lagrangian movements across the area is the knowledge of the instantaneous circulation. The roles of the barotopic tide and wind-induced vertical mixing have been evidenced through 1-D modelling studies (Altazin-Pichon 1981, Mariette 1982) and 2D ones (Mariette and Rougier 1982, Mariette 1985). However, the close connection between any enhancement of modelling and data analysis led Cochin (2006) to investigate the capability of ground wave high-frequency radars in the measurement of sea surface currents in the Iroise Sea over the SURLITOP (2005) experiment. Then, this author checked these sets

of experimental data against simulation data from a modelling with low-resolution or schematic atmospheric forcing. It showed the limits of applying such atmospheric forcings to the modelling of the Iroise Sea.

Thus, the combination of state-of-the-art ocean modelling and high-resolution meteorological forcing is needed in order to investigate more thoroughly the acknowledged patterns of the regional circulation and to study them in the light of the full three-dimensionality of the physical processes at work.

Here, to assess how the circulation calculated by a regional ocean model (MARS 3D) is affected by the quality of meteorological forcing we will, at first, briefly describe the main atmospheric and oceanic processes in action within the area of focus before introducing the numerical tools used in this study. This paper is organised around some specific experiments concerning the resolution of the meteorological forcing and the quality of the sea surface temperature employed to compute them.

The meteorological situations were simulated with the regional meteorological model, WRF.

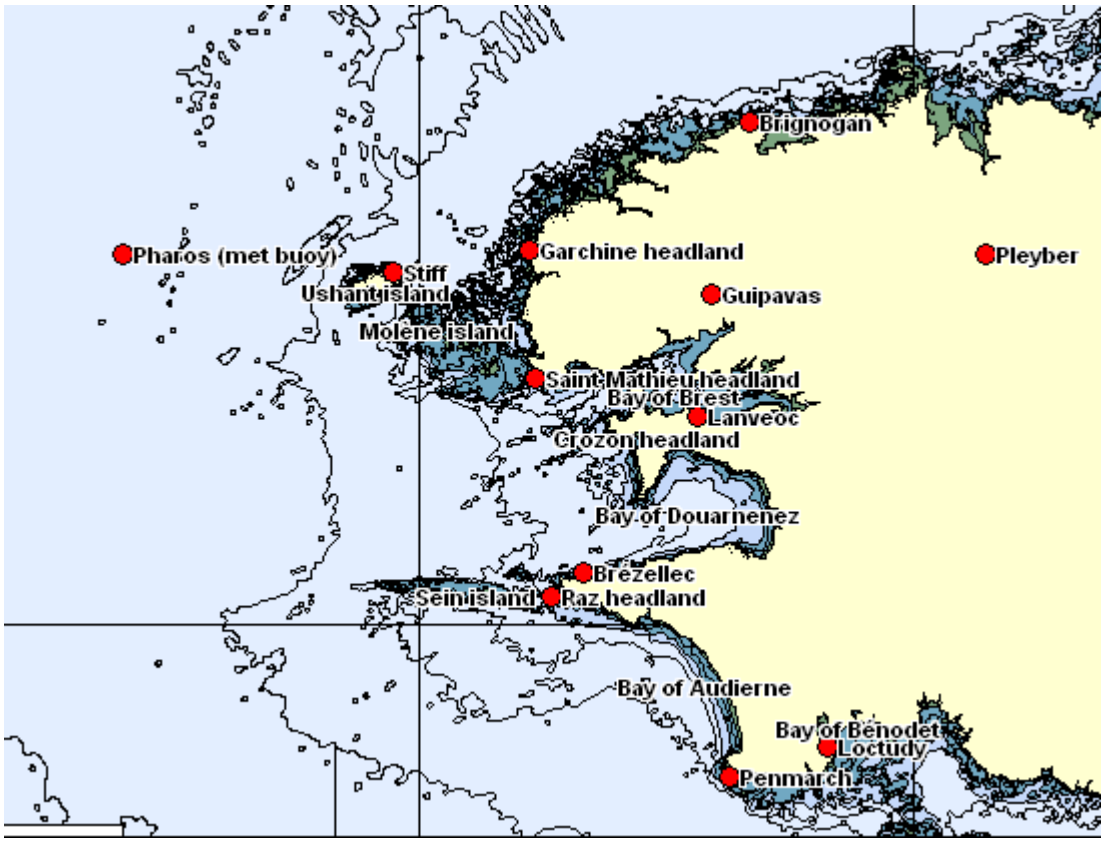

Fig. 1. Map of the Iroise Sea and Finistère

2 Area under study and numerical models

2.1 The Iroise Sea

2.1.1 Meteorological conditions

This study was focused on the summer and early autumn of year 2005. According to Météo France, this year was slightly warmer (about 0.5°C) than usual (see

www.meteofrance.com). The wind roses (Fig. 2) at Ushant (see map, Fig 1) show the directions of the prevailing winds according to their intensity between from July 1 and November 15. During this period, the weakest winds blew from the North North-East and North North-West; the former corresponds to anticyclonic weathers common in this area in summer and early autumn, whereas the latter is characteristic of low-pressure weathers. As far as middle- to intense-winds are concerned, the prevailing directions were North North-West, North-East and South South-West. If the North-East wind conditions belong to an anticyclonic regime, the South and North-West wind conditions are characteristic of mid-latitude depressions (West weathers and North-West to North weathers). The strongest winds blew from the South South-West and, to a lesser degree, from the North North-West during low-pressure episodes observed especially at the end of the period.

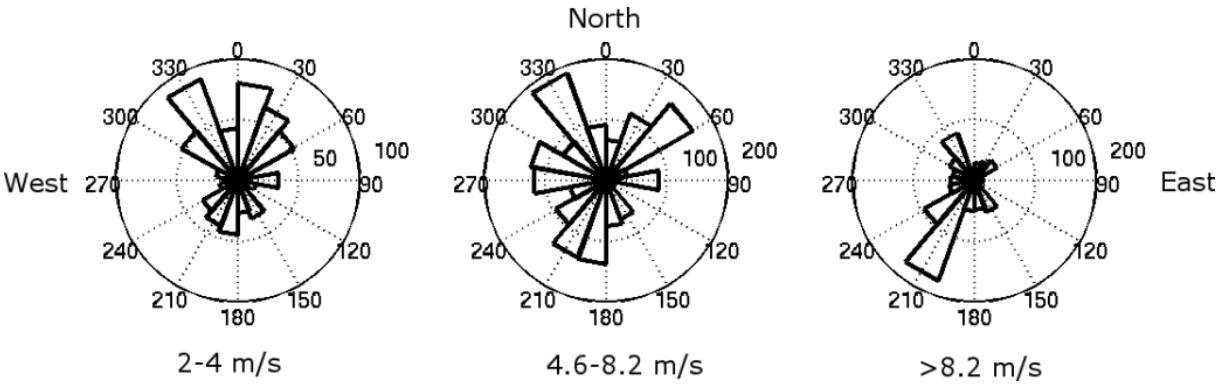

Fig. 2. Wind roses (in hours) from July1 to November9, 2005 at Ushant

Besides these synoptic features, small-scale effects take place in the closeness of topographic variations and over the sea, where horizontal thermal gradients are strong. Sea Breeze is also common in summer.

2.1.2 Dynamics and thermodynamics

The thermal structure and hydrodynamics of the Iroise Sea are mainly affected by mechanisms dependent upon the tide, wind forcing and density variations induced by both buoyancy fluxes at the sea surface and large-scale ocean variability. Considering the interactions between these different processes in addition to their individual contributions is also essential.

The main tidal contributions are M2, S2, N2 and K2 and diurnal components. By friction on the ocean bottom strong tidal currents induce the production of turbulent kinetic energy, which in turn generates an intense turbulent mixing. According to Le Cann (1982), in deep areas where the currents are weak like, for example, the southern Iroise Sea, the tidal mixing does not reach the surface and does not stand in the way of stratification during the spring warming period when the seasonal thermocline is developing; on the other hand, in shallow areas where the currents are strong, e.g. northern Iroise Sea, stratification is unable to develop because the whole water column is well mixed and homogeneous throughout the year. The tidal fronts are located at the interface of these areas.

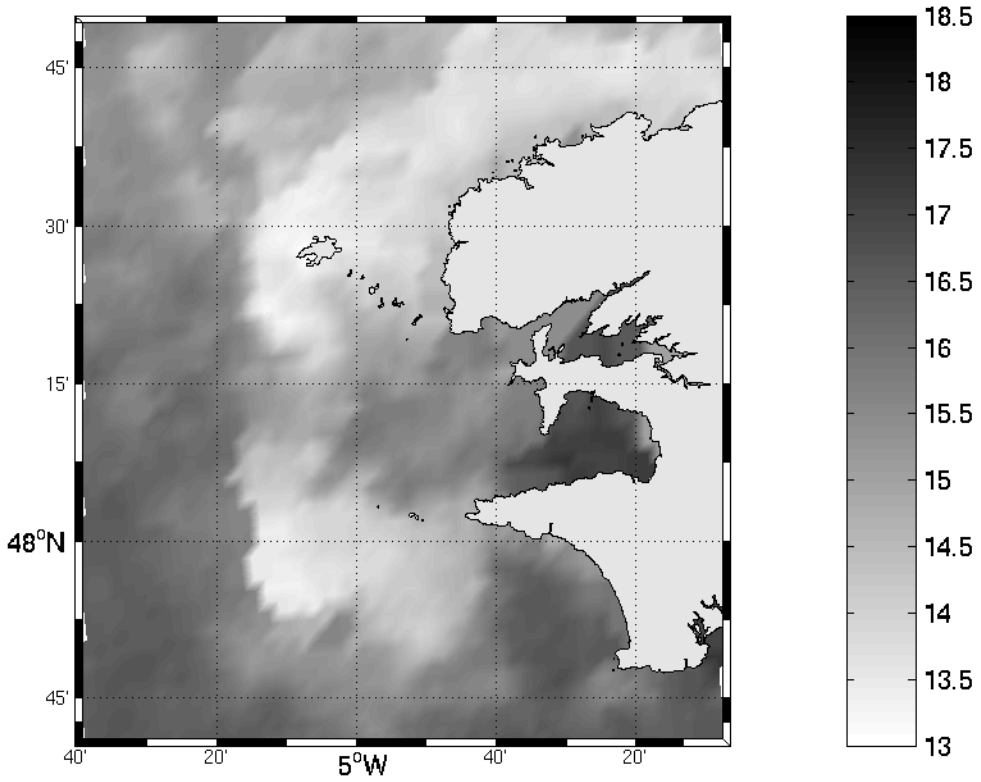

Fig. 3. Sea surface temperature, satellite map June 13, 2003 20:00UTC.

Figure 3 shows two fronts: the former, denoted here Ushant front, is a tidal front, whereas the internal one, at the verge of the system made by the bays of Douarnenez and Brest, is an estuarine front. Ushant front is located a few kilometres off Ushant island and gets closer to the coast near Raz headland (Pingree 1977, Mariette, Le Corre 1982). The horizontal thermal gradient is very strong and reaches 4°C in less than two kilometres. Two cold areas around Ushant and near the reef of Sein can be observed (Liam Fernand, 2003 Research Vessel programme including several cruises in the Western English Channel, personal communication). They are vertically homogeneous and can blend during strong sea states or spring tides. Between them, the intermediate area (14-15°C) is sometimes vertically homogenous. On its western side, it is separated from warmer offshore waters (17°C) by the thermal Ushant front, whereas on its eastern side, it is isolated by a thermohaline front from the warmer waters of the Bay of Douarnenez (17-18°C) where currents are weaker (Le Fèvre and Grall 1970). This internal front isolates warm and slightly salted coastal water from colder, homogeneous, saltier waters (Birrien 1987).

The influence of the seasonal warming was illustrated by measurements made by Morin (1984) in summer in the Bay of Douarnenez, that is on the eastern flank of the internal front: he, indeed, found a difference in vertical temperatures of more than 4°C and a bottom temperature above 13°C; on the other hand, vertical variations of only about 1.5°C were measured in the area between the two fronts. Therefore, such a vertical temperature gradient gives evidence of the occasional stratified nature of the intermediate area. Indeed, this intermediate area is not permanently homogeneous, and stratification can take place according to tidal phases and wind conditions.

The bays of Douarnenez and Brest are not only under the direct influence of the rivers, Elorn and Aulne, but also feel the remote flow of the Loire, whose mouth is located

much further South East). These provisions of fresh water specify the haline characteristics of the internal front of the Iroise Sea (Birrien 1987).

In the Ushant frontal area, a current directed along the tidal front and a secondary cross-front circulation driven by vertical diffusion can develop. These quasi-geostrophic currents create some baroclinic instabilities, which contribute to horizontal dispersion (Mariette 1983). It ensues that the geometry of the frontal area boundary is complex, and cyclonic eddies are frequently observed (Birrien 1987). The wind acts on the front structure because of the transfer of turbulent kinetic energy from the atmosphere to the ocean and of the enhancement of mixing in the surface layer. In the Iroise Sea, heat fluxes also play a determining role in the development of the frontal structure. In the sunny days of spring, heat is stored by the ocean, and a homogeneous warm water layer lies above the thermocline, which settles at depth within 10 and 60 m. This thermal profile disappears in autumn with the strong winds and associated heat losses.

The above-mentioned thermal structures are permanent in summer, but their extent and intensity both fluctuate with the amount of energy exchanged at the air/sea interface and with the range of tide. Thus, the wind-generated friction allows the thermocline to deepen and the sea surface temperature (SST) to get colder. The effect is the highest in winter when the whole water column is mixed and cooled down because of emphasised winds and heat losses. Indeed, the stratification of the column is intimately connected with the vertical extent of the surface and the bottom mixed-layers.

Non-linearity associated with tidal current fluctuations creates a residual circulation whose intensity and direction are also sensitive to the local atmospheric forcing (wind and heat fluxes) and larger-scale density variations. Moreover, the residual currents are strongly implicated in advection. The neap/spring tide cycle and atmospheric forcing may affect the location of Ushant front by moving it up to 4 km away from its average position (Altazin-Pichon 1981).

To gain more insight into the key-role of meteorological forcing on local dynamics (surface current deviation, advection, modification of density-driven currents, upwelling processes) and thermodynamics (front displacements, thermocline deepening), our investigations were focused on the way a system using a regional atmospheric model has to be adjusted in order to force a regional ocean model of the Iroise Sea. Moreover, in the case of such frontal structures, it sounded us worth discussing the usefulness of refining air/sea exchanges in regional modelling to better describe vertical mixing.

2.2 Atmosphere and ocean models

2.2.1 The regional meteorological model, WRF (Weather Research and Forecasting model)

WRF belongs to a new generation of mesoscale models used to forecast and simulate the atmospheric circulation (Klemp et al. 2000, Wicker et al. 2002, Skamarock et al. 2005). This 3D and non-hydrostatic meteorological model is based on the equations of mechanics for a fully compressible fluid and of thermodynamics. The computed parameters are the horizontal and vertical wind components, the air temperature and relative humidity, the atmospheric pressure as well as the downward short-wave and long-wave fluxes at the ground surface. Among them, the downward long-wave flux at the ground surface is the only one that takes into account the cloud cover fraction; it uses a land-following, hydrostatic pressure and vertical coordinate set at the constant value of 1013 mb over the highest model level.

The physical options of WRF used in the configurations of concern here have been classified into several categories: microphysics (Ferrier 2002), cumulus parameterisation (Janjic 1994, 2000), long-wave radiation (GFDL scheme, Fels and Schwarzkopf 1975, Schwarzkopf and Fels 1991), short-wave radiation (GFDL scheme, Lacis and Hansen 1974), planetary boundary layer physics (Mellor-Yamada-Janjic TKE planetary boundary layer scheme, Janjic 1990, 1996, 2002), surface layer physics (Janjic 1996, 2002), land surface physics (Noah land surface model, Chen and Dudhia 2001). Prior to the description of the time changes occurring in the atmospheric circulation, WRF needs to be fed with meteorological data and static ones; the latter deal with the topography, vegetation, water and soil types. In this study, the default horizontal resolution of the global data about topography, land use and soil texture is 30 seconds of latitude (~925 m). The resolution on the soil temperature is about 1 degree in latitude (~111 km), whereas those on vegetation and albedo data are alike and of about 10 minutes of latitude (~18.5 km).

The meteorological data necessary for model initialisation and boundary conditions are wind components, potential temperature, pressure and moisture; all of them come from the 6-hour NCEP global tropospheric analyses available on a global 1 x 1 degree grid. These global data are introduced in the model by a relaxation method (Davies and Turner 1977). For the boundary condition over the ocean, we also used an atlas of SST corresponding to a 10-day climatology with a 9-km resolution calculated on using night data from NOAA satellites from 1985 to 1995 (Faugère et al. 2001).

Figure 4 shows the two geometrical configurations used in this study. The first of them is a single 20-km grid. On the other hand, the second one is more complex because it consists in a two-way active nested run with two grids whose resolutions are 18 and 6 km, respectively. The period under study extends from July to November 2005 with a sampling period of about one hour for the output. Both configurations have 28 levels. The total number of computation points is 91 x 91 x 28 for the 6-km grid.

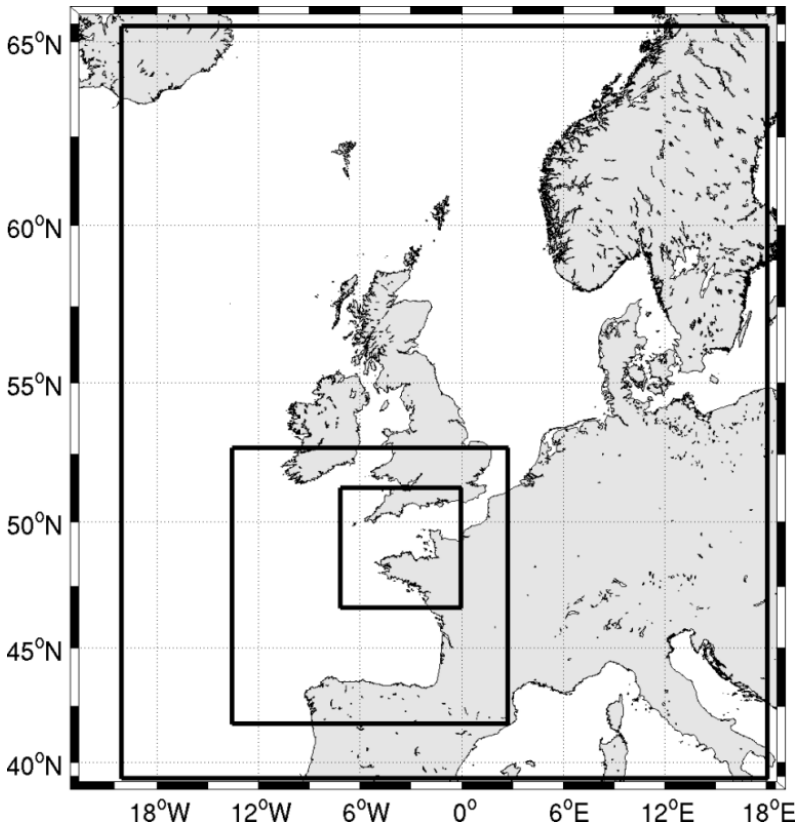

Fig. 4. 20-km WRF configuration and 2-grid nesting WRF configuration (18 and 6 km)

2.2.2 The regional oceanic model, MARS (Model for Applications at Regional Scale)

The numerical model of coastal hydrodynamics, MARS, is a 3D code developed within IFREMER (Lazure and Dumas, accepted in Advances in water resources). It relies on the hydrostatic approximation and the Boussinesq hypothesis and computes ocean physical variables (temperature, salinity, currents and free surface elevation) from the solutions of primitive equations. Moreover, it uses sigma coordinates on the vertical, and time integration is based on a time-splitting method in order to calculate independently the fast and the slow baroclinic modes. The turbulent closure scheme is the TKE model proposed by Gaspar and co-workers (1990); it is used to parameterise the vertical turbulent viscosity and the diffusion coefficients; as these parameters are computed on using the Laplacian proposed by Smagorinsky (1963), they depend on the local mesh dimensions and velocity gradients.

The bathymetry used in this study (Fig. 5) came from a 500-m resolution SHOM (French naval hydrographic and oceanographic service) database. The bottom friction was parameterised with a quadratic formulation. The drag coefficient is a function of the roughness length, z_0, set constant and equal to 3.5 mm; its literal expression is $C_D = (\frac{\kappa}{\ln \frac{h}{z_0}})^2$, where κ is the Von Karman constant (0.4), and h is the height of the whole water column. In the experiments analysed in this study, the atmospheric fluxes were computed with bulk formulae (Luyten 1992) applied to WRF outputs. Thus, the latent heat flux and the sensible heat flux were calculated with bulk formulae involving the 10-m wind components, 2-m air temperature and relative humidity. The short-wave radiative flux and the long-wave radiative flux, which takes into account cloudiness, were directly entered in MARS on considering the albedo correction and the radiation of the sea surface. The quadratic parameterisation reported by Geernaert and co-workers (1986) is used for surface friction with a drag coefficient defined as $C_d = 0.001 \times (0.43 + 0.097 \times windspeed)$. Initial conditions for tracers are taken from a previous simulation computed under the same conditions, but starting from a winter homogeneous situation. As far as boundary conditions for tracers are concerned, when velocity is inwards-directed, the horizontal gradients for temperature and salinity are null. When velocity goes outwards, tracer values at the boundaries are imposed by the advection of the internal values.

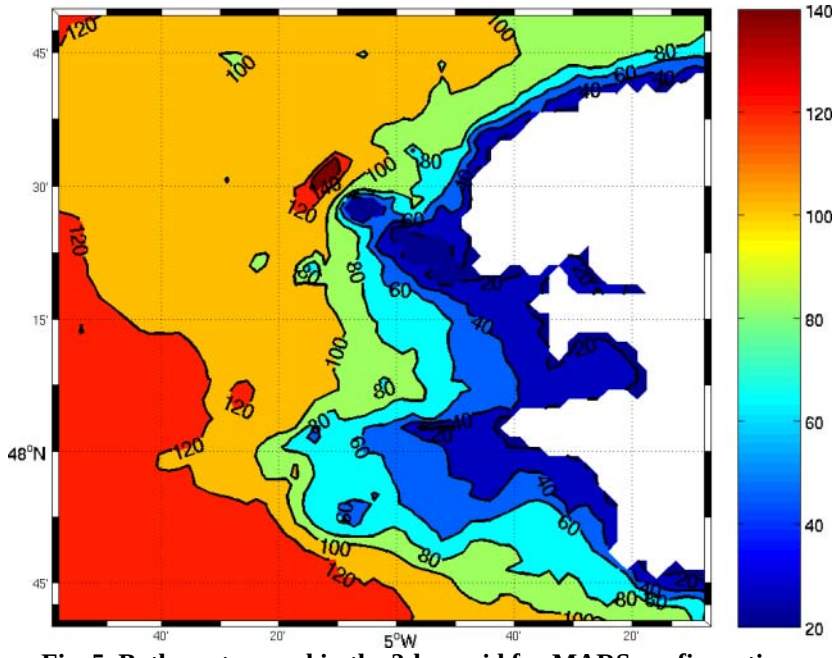

Fig. 5. Bathymetry used in the 2-km grid for MARS configuration.

Our 3D model of the Iroise Sea is embedded in a 2D coarse resolution model. The open boundary condition for sea surface height in the 3D model is provided by the 2D barotropic model, which is itself forced by the sea surface height from the FES (2004) global tidal model with 8 tidal components (M2, S2, N2, K2, P1, O1, K1, Q1) (Lefèvre 2002). For the 3D model, the velocity gradients are equal to zero at the open boundaries. This hypothesis is justified by the slight variations of tidal currents on the abyssal zone. The configuration under study consists of a 5-km-resolution 2D model where a 2-km 3D model with 96 x105x30 computation points is embedded (Figure 6). The area of concern in this study indicated by the smaller rectangle on Figure 6 is a sub-domain of our 3D model.

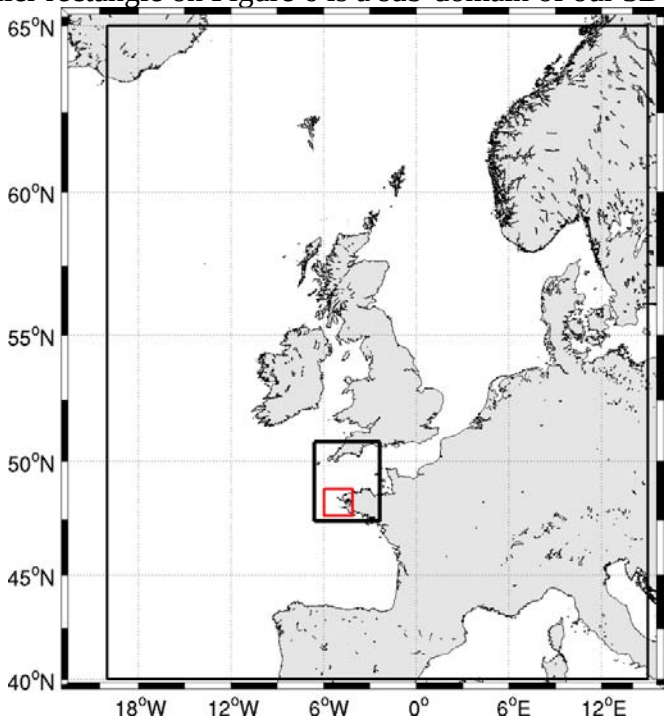

Fig. 6. 2-grid MARS configuration with the zoom for the area of study. (the smallest rectangle: sub-domain of 3D model, middle rectangle: 3D model, the biggest rectangle: 2D model)

3 Impact of high resolution forcing on Iroise Sea modelling

It is worth, now, focusing on the study of the ocean response to specific meteorological forcing by checking, at first, the results issued from WRF against genuine atmospheric data. To gain more insight into the impact of the quality of the different meteorological forcings on Iroise Sea modelling, we will compare our reference simulation of the Iroise Sea run with a high-resolution atmospheric forcing to three other ocean experiments forced with less precise atmospheric fields.

3.1 Atmospheric fluxes simulated by WRF

3.1.1 Comparison with ground data

Before carrying out the analysis of WRF-run numerical situations it is worth comparing observations against results taken from the 6- and 20-km WRF configurations, over the period from July 1 to November 15, 2005. Moreover, the scarcity of real data made us focus the validation of simulation results on the wind. Nevertheless, some additional meteorological parameters needed for the calculation of heat fluxes between the atmosphere and the ocean come from records, over the same period, by a meteorological buoy (48.5°N, -5.6°W) positioned in the middle of the Ushant traffic separation scheme.

To summarize, the datasets available on site for the Iroise Sea are:

- analysis charts from the UK Met Office;
- 2-m air temperature, 10-m wind data, 2-m relative humidity and surface pressure from the met buoy belonging to Météo France (see Fig. 1);
- 10-m wind data from seven onshore meteorological stations (Brignogan, Raz, Ushant, Guipavas, Lanvéoc, Penmarch, Pleyber) belonging to Météo France (see Fig. 1);
- wind direction series (August to November 2005) coming from high-frequency radar data, with a spatial resolution of about 1.5 km and a temporal resolution of about 20 mn.

Hereafter we will, at first, check our WRF synoptic scales against the UK Met Office analysis charts, then the smaller scales against specific meteorological stations and coastal radar observations.

UK Met Office Analysis Charts

A visual comparison of the results from the 20-km WRF configuration used to take into account large-scale atmospheric patterns against the UK Met Office Analysis Charts available for the period of study evidenced the correct reproduction by WRF of the large-scale features.

On July 21, an anticyclone was located off the coasts of Brittany (Fig. 7a). A comparison of the isobars map from WRF (Fig. 7b) with the analysis chart from the UK Met Office (source: The Deutsche Wetterdienst in Germany) shows that WRF clearly reproduces the synoptic scales observed on that day. Moreover, the WRF-forecasted wind direction is northwesterly winds over the Iroise Sea in agreement with the Buy Ballot law (in the Northern Hemisphere, surface winds blow clockwise around and slightly out of a surface high because of friction). On July 24, a low atmospheric system passed over the Iroise Sea; the analysis chart about the same day (Fig. 8a) shows a warm front and a cold one on either side of the Iroise Sea, which are both clearly reproduced by WRF with strong southwesterly to westerly winds (Fig 8b).

Confrontation of all available analysis charts for the period extending from July 1 to mid-November, 2005 against WRF isobars maps led us to conclude that the meteorological situations were alike in both sources.

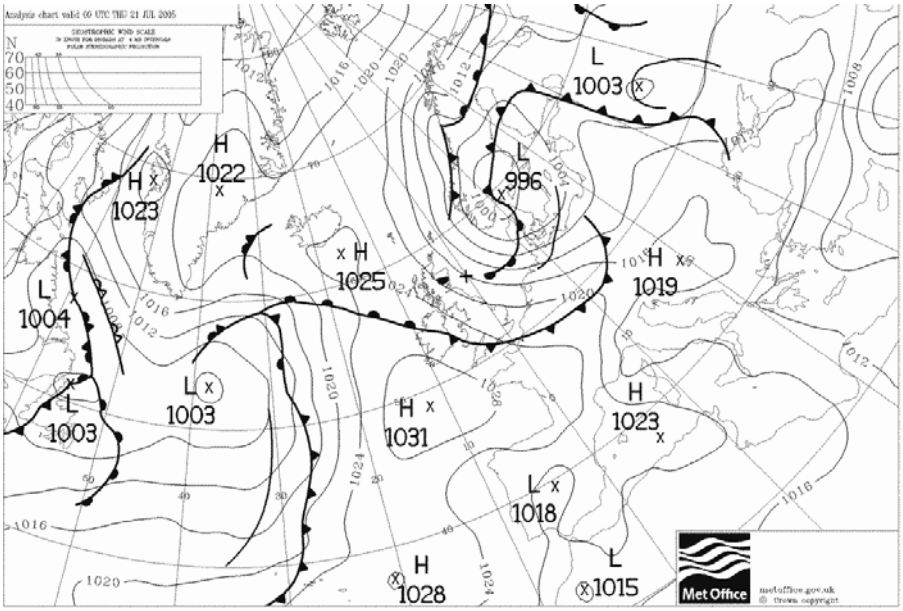

Fig. 7(a). Analysis chart July 21, 2005, 00 UTC (from http://www.wetterzentrale.de/topkarten/fsfaxsem.html)

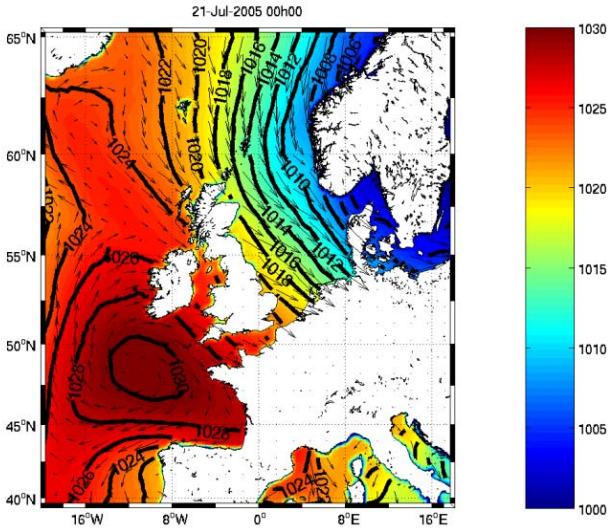

Fig. 7(b). WRF surface pressure in (hPa) and wind.

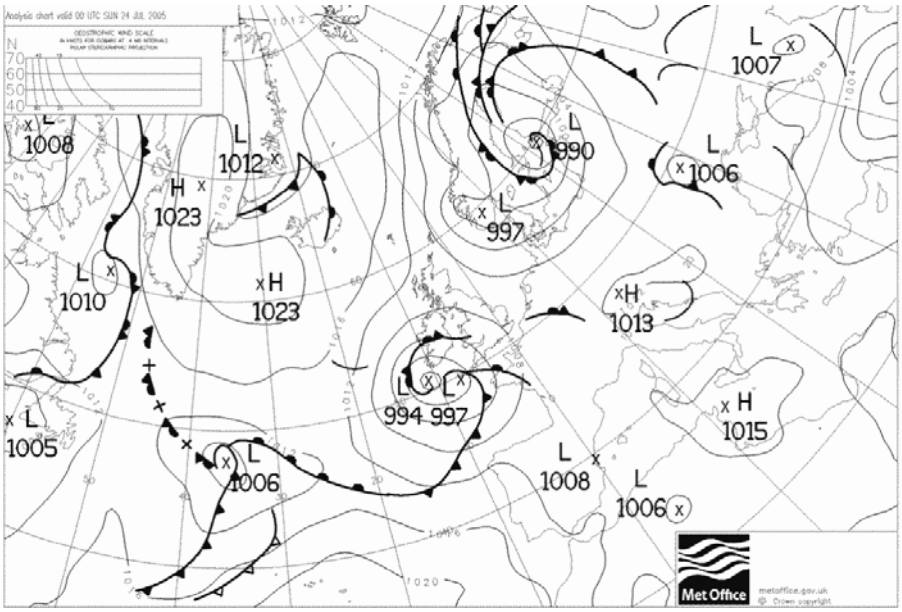

Fig. 8(a). Analysis chart July 24, 2005, 00 UTC (from http://www.wetterzentrale.de/topkarten/fsfaxsem.html)

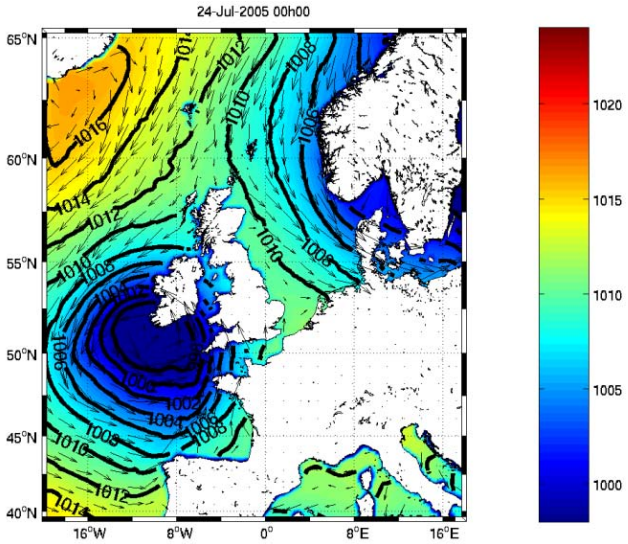

Fig. 8(b). WRF surface pressure (in hPa) and wind between the passages of the warm and cold fronts.

Met buoy and onshore meteorological station data

In the following, the WRF results considered for spot comparisons with ground data are those issued from the 6-km WRF configuration, and the measure points are the met buoy, Guipavas and Ushant because of the relevance of their geographical positions.

As far as wind is concerned, scatter plots show an acceptable linear correlation between modelled and observed values with coefficients close to 0.9 for direction and intensity (Figs. 9a,b).

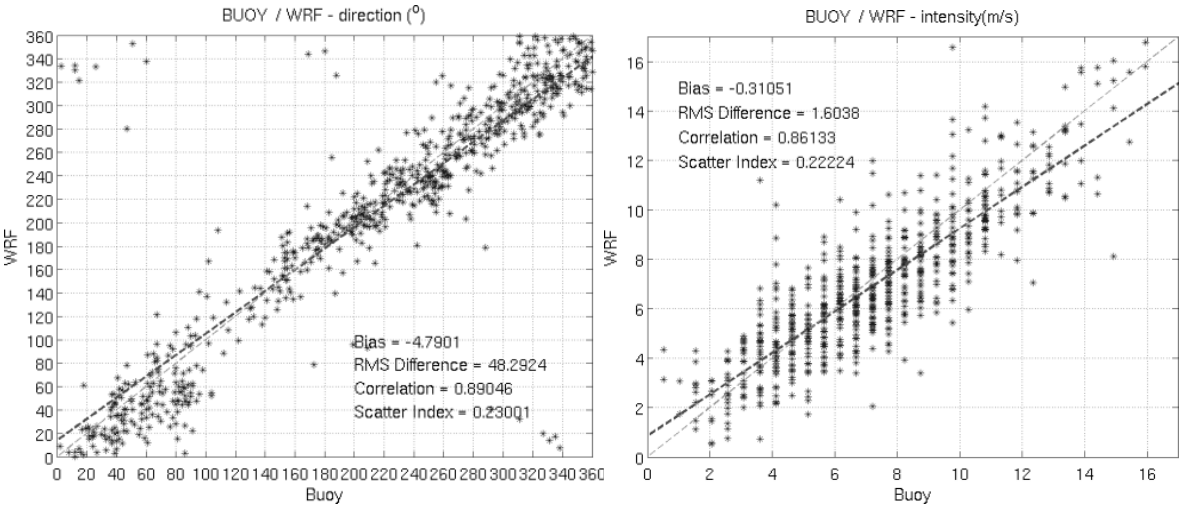

Fig. 9. Correlation between WRF and met buoy for (a) wind directions and (b) wind intensities.

Let X and Y be two variables of the same nature, Scatter Index is defined as $SI = \frac{RMSE}{\overline{X}}$ where $RMSE$, the Root Mean Square Error, is defined as $RMSE = \sqrt{\frac{\sum_{i=1}^{N}(X_i - Y_i)^2}{N}}$ and $\overline{X}$ is the average of X. For the met buoy, Guipavas and Ushant, scatter indices are generally around 0.2.

About the wind intensity, one should note that WRF overestimates weak winds (around 5 m/s and below) and underestimates winds of speed exceeding 5 m/s (Fig. 9b).

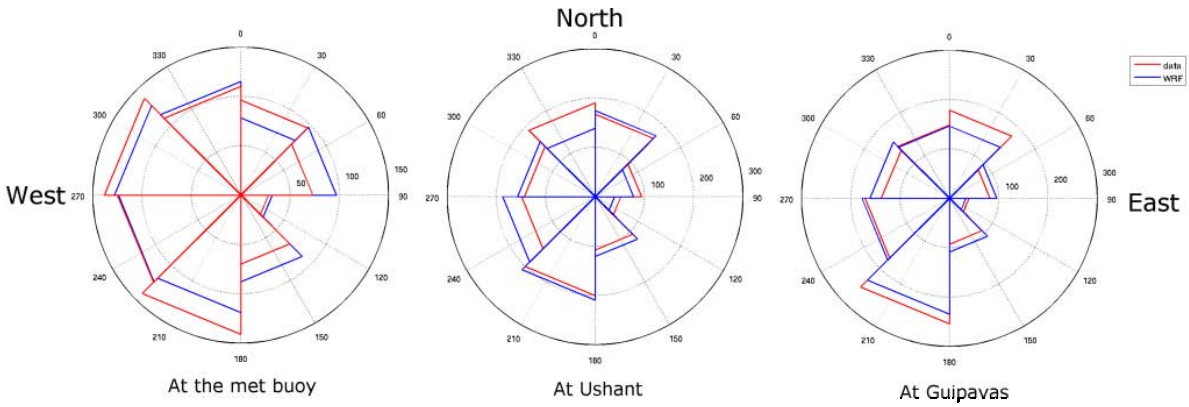

Fig. 10. Distribution of wind directions at the met buoy, Ushant and Guipavas, respectively.

For the directions, the compass card at the met buoy shows that the occurrence frequencies of wind according to its direction are well reproduced by WRF over the period under study, especially for northeasterly, northwesterly and East South-East winds (Fig. 10). At Guipavas, westerly winds are usually better reproduced than easterlies, likely because of the position of the meteorological station. Indeed, at this inland location, the westerly fluxes, which are pure synoptic fluxes, have met no obstacle along their travel to the weather station, whereas northeasterly fluxes have been affected by the geometry of the coast and land

topography. At Ushant Island, the asymmetry in wind direction frequencies is also correctly reproduced in WRF results; the model tends to slightly shift the direction of the incoming winds to the West. Finally, the best-reproduced wind directions are South and northeasterly. As the meteorological station is located on the east side of the island, westerly fluxes are likely disturbed by the coast. Actually, the whole point of using such a meteorological model is to account for orographic effects; but because of the very coarse resolution of the soil temperature data; WRF may fail to exactly reproduce small-scale effects at the right time. Moreover, the resolution of WRF outputs may be too coarse for these phenomena. In our opinion, overall trends in wind-frequency and -intensity variations are fairly reproduced by WRF at the three weather stations.

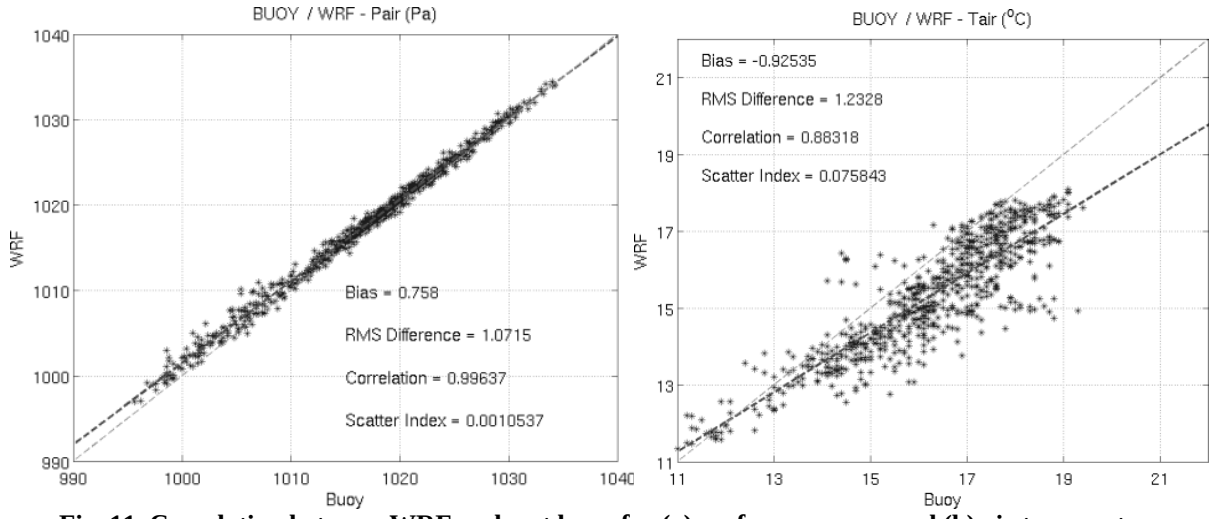

Fig. 11. Correlation between WRF and met buoy for (a) surface pressure and (b) air temperature.

About the surface pressure data, the correlation found by computation between the WRF- and met buoy-data is illustrated in Fig. 11a; the correlation coefficient and scatter index are about 0.99 and about 0.1%, respectively. The quality of this meteorological parameter and those of the boundary conditions and topography are closely related: so, provided that the large-scale meteorological conditions, which are the main contribution to the pressure field, be well-captured by the boundary conditions, it is very likely that the computed pressure field will be nearly the true one. But, one should be aware that the presence of small-scale structures in the pressure field is not excluded by such results. On the other hand, WRF underestimates the surface air temperature (bias of about –0.9°C on Fig. 11b) despite the correct reproduction of its variations (correlation coefficient of about 0.88 on Fig. 11b). Since SST plays an important role in the stability of the low atmospheric layers, these experiments suggest that the temporal and spatial resolutions of the SST data used to force the model may be too coarse to reproduce the correct order of magnitude for the air temperature.

Relative humidity is a diagnostic variable determined from WRF results through the computation of the air temperature, surface pressure and mixing ratio. The correlation between our simulation results and observations determined from the scatter plot of relative humidity was found to be about 0.7. The bias of about 6% due to the constant underestimation of this parameter by WRF is likely partly attributable to the bias on the computed air temperature. However, the main contribution is undoubtedly the reliability on the WRF-computed water mixing ratio, but it is uneasy to verify with ground data. This problem of relative humidity is recurrent in meteorological models.

In conclusion, further to these comparisons of numerical results from WRF against localized measurements, the reproductions by WRF of surface pressure, air temperature and wind components are reliable. But, as the computation of relative humidity remains difficult, the thermodynamics of the Iroise Sea in a regional ocean simulation is likely impaired by the difference between modelled and observed values.

HF radar data

We used the high-frequency radar dataset to extend our validation over a large subdomain of the regional model. Figure 12 illustrates the results of the comparison between wind directions calculated by WRF and observed by the radar system. It shows that the linear correlation found from calculation between both fields is rather low around the islands because of either a lack of radar resolution in this area, or a shadow effect by the islands. It is worth noting that, offshore, the correlation coefficients are close to, or greater than, 0.85.

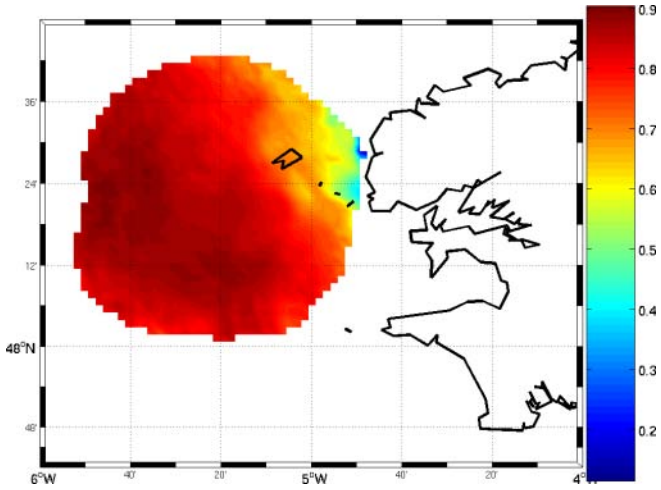

Fig. 12. Correlation map between WRF results and HF radar data from August to mid November 2005.

The scatter plot calculated at (48.3 N;-5.4W) (linear correlation of about 0.85) gives a scatter index of roughly 0.3. It also highlights the inability of WRF to give reliable reproductions of south-southeasterly winds. In addition, some northeasterly winds in HF radar data are simulated by WRF as north-northeasterly winds, which confirms the trend shown by WRF to shift wind towards westerlies.

Figures 13a and 13b give a snapshot of a Northeasterly flux episode; WRF represents quite well the overall direction of the wind, but as far as small-scale features are concerned, the model is unable to capture all of them. For instance, our WRF configuration gives no reproduction of the North flux between Ushant and the Finisterian coast. The solution to eliminate such a bias is likely a better resolution of WRF outputs.

The comparisons of WRF results against field data proved its ability to reproduce large and small-scale features present in the wind field. On the other hand, for the other meteorological parameters they highlighted some deviations, which are of the same order of magnitude as those obtained with other meteorological models. It is also worth noting that the quality of reproduction of these parameters is deeply linked to the overall quality of the sea surface temperature data used to force the model.

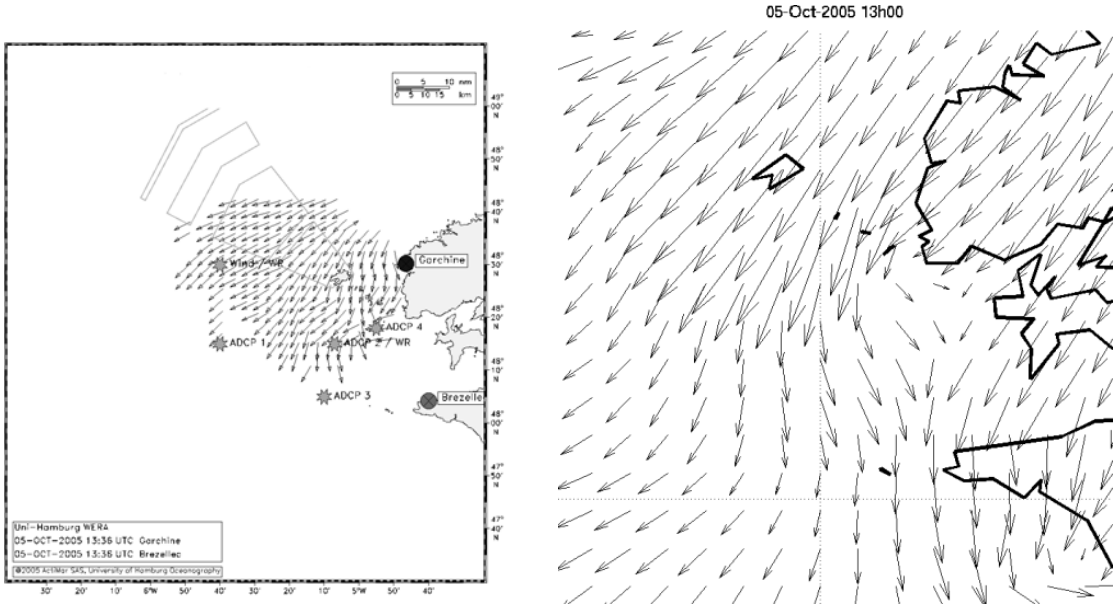

Fig. 13(a) Wind directions estimated by HF radars on October 5, 2005 13:36 UTC, (b) WRF wind field on October 5, 2005 13:00 UTC.

3.1.2 Meteorological parameter sensitivity to mesoscale SST patterns

The small-scale phenomena introduced on the meteorological fields by changes in surface temperature and coastal geometry may, in the end, produce a noticeable signature on the surface ocean dynamics. It thus sounded us worth investigating this feature from the results of our 6-km WRF configuration.

The observation of temperature variations of about 4°C in less than 2 km in the frontal structures characteristic of the weather of the Iroise Sea in summer led us to wonder about their impact on meteorological parameters.

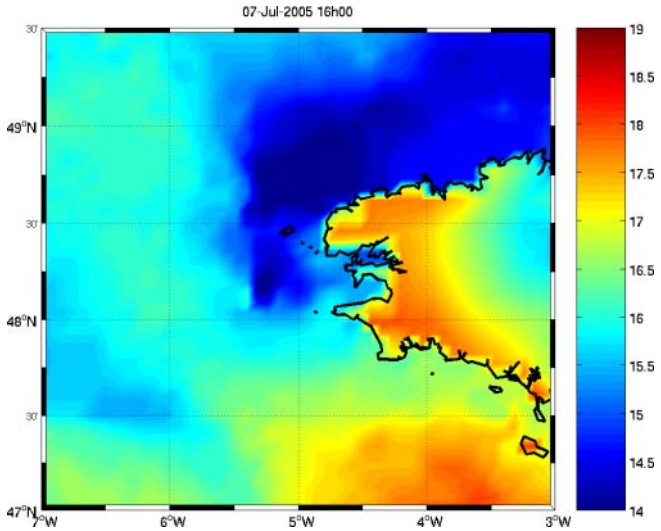

Fig. 14. Sea surface temperature (in °C) used as WRF boundary conditions.

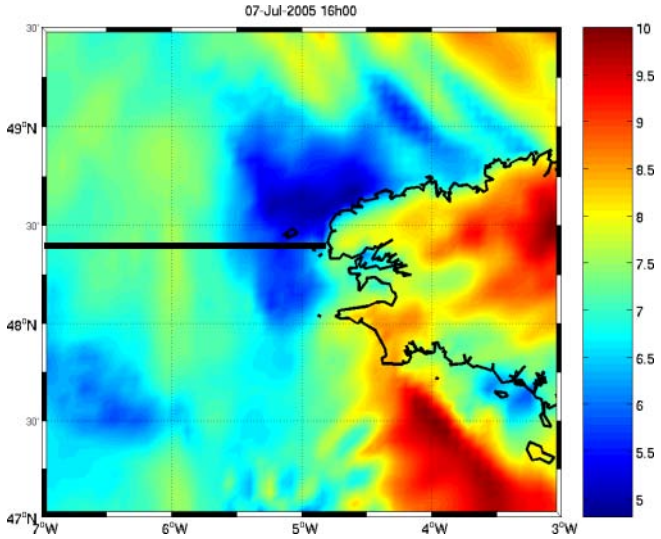

Fig. 15. WRF wind intensity (in m/s), July 7, 2005 16:00 UTC.

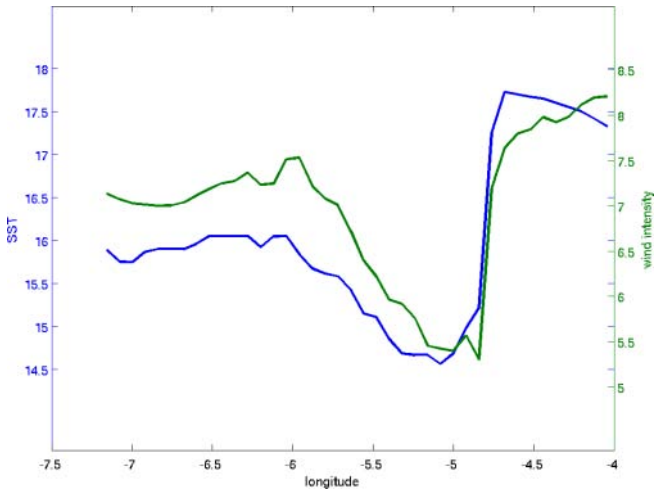

Fig. 16. Superimposition of wind intensity (in m/s) and SST (in °C) along the black section (see Fig 15).

At this stage, it is worth recalling that, in this study, the regional meteorological model was forced by a 10-day climatology of the sea surface temperature with a resolution of 9 km (WRF1), which had some consequences on the wind simulation. Indeed, strong horizontal gradients in SST (see Figure 14) can lead to local small-scale wind structures. For instance, velocity gradients may appear in the horizontal wind components when seasonal fronts are developing across the Iroise Sea. The WRF-reproduced wind field (Fig. 15) exhibits the Ushant and internal fronts observed during the anticyclonic episode of July 6 and 7; the resulting difference in wind intensities is 3 m/s with a lower value over homogeneous cold water than over stratified water columns. The superimposition of the sea surface temperature and the wind intensity versus the longitude along the section crossing the Iroise Sea (Fig.16) indicates that, offshore, where the sea surface temperature is close to 16°C, the wind intensity is about 7.5 m/s. Along the coast, the SST and wind intensity are both dropping down . Finally, when the SST is increasing at the entrance of bays, the wind gets stronger. The air column is really stable over cold water and unstable over warm water. It is worth noting that the wind tends to make uniform maritime areas; in a way, it gives stability to the region. Synoptic conditions on July 7, with moderate breeze effects, were optimal to observe this

phenomenon. Such observations highlight the interest of atmosphere - ocean couplings for regional coastal modelling studies.

It is also worth focusing onto the air temperature and relative humidity spatial distributions on July 7. Figure 17a shows the similarity between both spatial distributions, but with a less contrasted pattern for the air temperature than for the sea surface temperature. As far as relative humidity is concerned, its rate is higher over the homogenous area of the Iroise Sea than offshore (Fig. 18a). Indeed, at equal quantities of water vapour, relative humidity is increasing when temperature is lowering. These spatial distributions of air temperature, wind speed and relative humidity show obvious correlations with the spatial variations of sea surface temperature.

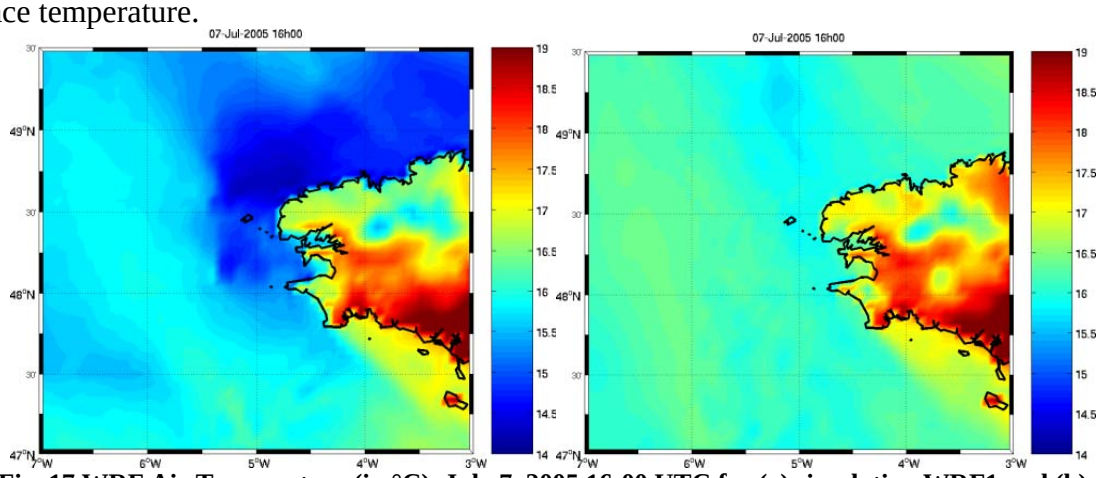

Fig. 17 WRF Air Temperature (in °C), July 7, 2005 16:00 UTC for (a) simulation WRF1 and (b) simulation WRF2.

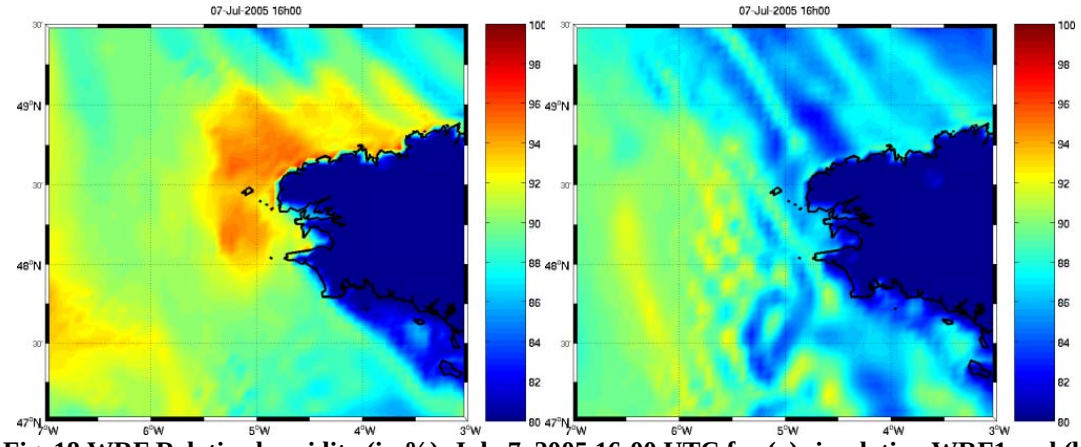

Fig. 18 WRF Relative humidity (in %), July 7, 2005 16:00 UTC for (a) simulation WRF1 and (b) simulation WRF2.

Thus in the case of the Iroise Sea modelling, a prerequisite to a realistic production of atmospheric fluxes by any atmospheric model is to take into account the data relative to the surface temperature. A proven evidence of the relevance of updating the sea surface temperature in meteorological forcing computation is given by a comparison of the results from a WRF simulation forced with a spatially-uniform sea surface temperature issued from a spatial average of the 10-day climatology (WRF2) (Figs. 17b and 18b) with the WRF reference simulation results (WRF1).

To gain additional information to the hereabove observations, we tentatively quantified the effect of the sea surface temperature on air temperature, relative humidity and wind from the values measured at Pharos, the only measure point located within our study area (see Fig. 1). The influence of the sea surface temperature update is not so obvious as far

as the directions of the offshore wind are concerned. Indeed, offshore, the wind direction is governed by synoptic phenomena. But, updating the sea surface temperature to get a more realistic sea surface temperature enhanced the quality of the WRF-computed wind intensity: correlation between measured and computed wind intensities was about 2% better, the bias was reduced by 5%, the root mean square error and scatter index were also better. The impact of such a sea surface temperature update in WRF recalls the aforementioned accordance between the horizontal thermal gradient in the sea and the wind intensity gradient under calm meteorological conditions. But, we are aware of the limitations of this analysis because of the consideration of wind at 10 m over the sea surface. However, as far as the air temperature is concerned, the sea surface temperature update in WRF has a real impact according to the previous observations. Further to a comparison of WRF1 and WRF2 simulations, the correlation coefficient can be improved by 5% and the bias lowered by 50%. Similarly, for relative humidity, the correlation coefficient depends on the sea surface temperature dataset used and can be increased by 3% and bias by 20%.

To investigate the effect of the sampling of the sea surface temperature in the computation of meteorological parameters we compared the results, at Pharos, of the WRF2 simulation against those of a WRF simulation that took into account a spatially-uniform sea surface temperature with a daily temporal resolution (WRF3). This SST dataset for WRF3 simulation was built from daily satellite maps of sea surface temperatures (source: SAF O&SI: Satellite Application Facility Ocean and Sea-Ice, from EUMETSAT/Météo-France in Lannion). It showed that the temporal resolution (1 or 10 days) for sea surface temperature is less important than the spatial resolution, since correlation coefficients and biases for all meteorological variables between ground data and model results were of about the same order of magnitude. Nevertheless, we are aware that the location of our measure point, Pharos, offshore Ushant, far away from every local costal effect and also outside of the frontal area makes that these comparative analyses need to be cautiously handled. So, drawing conclusion about the temporal and spatial resolutions of the SST dataset used in WRF1, WRF2 and WRF3 remains difficult. The expected improvement in the meteorological forcing is rather near the coast and in frontal areas.

The relevance of updating the sea surface temperature dataset being obvious as regards the spatial distribution of air temperature, relative humidity and wind speed, it would be worth enhancing the quality of the used sea surface temperature dataset used by coupling atmospheric and ocean models.

Despite its limitations because of the lack of field data for validation of local phenomena this short sensitivity study about the spatial and temporal resolutions of the sea surface temperature used to force a regional meteorological model highlighted improvements in the quality of computed meteorological parameters. It also led us to wonder about the sensitivity of the ocean to these local coastal phenomena, and then to investigate the impact of high-resolution meteorological forcing upon the quality of our regional ocean modelling.

3.2 Dynamics and Thermodynamics simulated by MARS

3.2.1 Comparison with ground data

The meteorological forcing employed to compute the dynamics and thermodynamics of the Iroise Sea from July 1 to mid-November, 2005 is WRF1. For hydrodynamics, the datasets used for carrying out comparisons are:

- Surface currents measured by 2 HF radars located at Brézellec and Garchine headlands (SURLITOP experiment). The surface currents data are available every 12 minutes with a spatial resolution of about 2-km.

Those for thermodynamics are:

- 3D monthly climatology of temperature for the Bay of Biscay with a spatial resolution of about 0.1° of latitude and 261 depths from 0 to 4000 m (http://www.ifremer.fr/climatologie-gascogne/index.php).
- Sea surface temperature obtained from satellite data (source: SAF O&SI: Satellite Application Facility Ocean and Sea-Ice, from EUMETSAT/Météo-France in Lannion). The data used for this analysis are night satellite pictures (at 8:00 p.m. and 2:00 a.m.). At the sub-satellite point, spatial resolution is 1.1 km.
- Sea surface temperature coming from the "Pride of Bilbao" ferry, with a spatial resolution of 2 km and a temporal resolution of 20 minutes. (source: http://www.noc.soton.ac.uk/ops/ferrybox_2005/ferrybox_index_2005.php)

The following comparisons are based on the results from the 2-km MARS configuration. Moreover, they mainly deal with the sea surface physical variables (temperature and currents) in order to assess the impact of high-resolution forcing on the sea surface. Other comparisons with a monthly climatology of the temperature within the Bay of Biscay will be also discussed to check the vertical temperature structure computed with MARS;

Surface currents

In order to validate the WRF-simulated hydrodynamics, the statistical and harmonical analyses of the comparisons with HF radar surface currents were performed in the radar coordinate system and in the Cartesian coordinate system, respectively.

-Statistical analysis

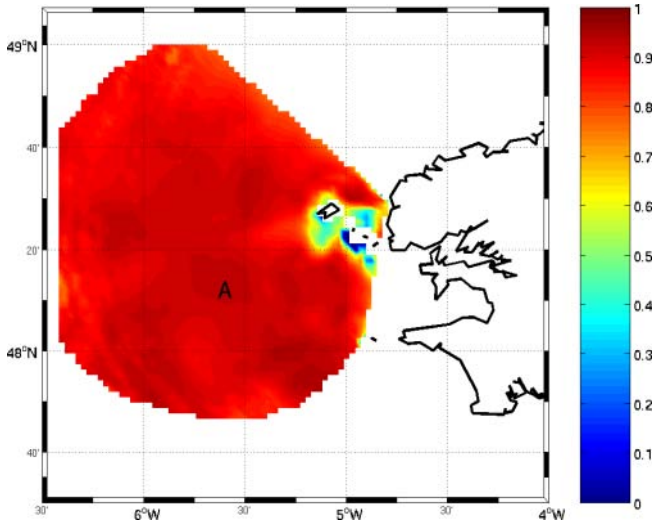

Fig. 19. Correlation coefficients between surface currents estimated by MARS and those measured with Garchine HF radar.

The two radars used for the SURLITOP experiment are located at Garchine and Brezellec headlands (see Figure 1). Figure 19 illustrates the very satisfactory correlation found between the radar surface current measurements (field data) at Garchine and the results

from MARS simulations; the correlation coefficient is about 0.9 in almost all of the area. Moreover, with a correlation coefficient of 0.93, a bias of 0.04 m/s and a root mean square error of 0.15 m/s the scatter plot at the point, A, gives evidence of the quality of coherence between field data and simulation results. The reliability of radar measurements in the vicinity of islands is impaired by shadow effects, which drove us to discard the correlation near the islands of Ushant and Molène.

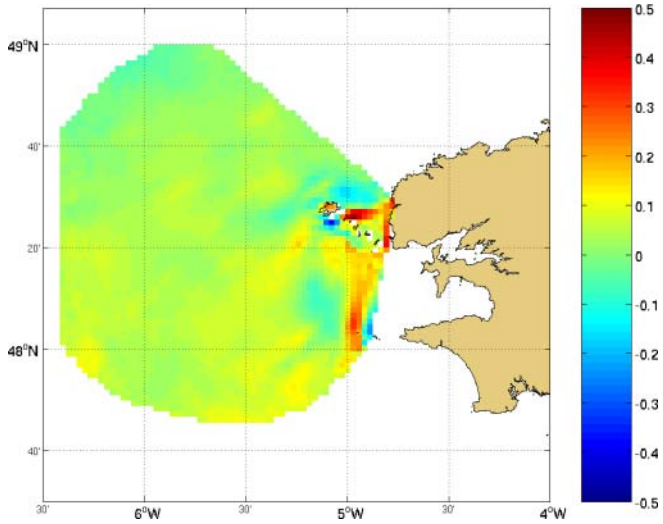

Fig. 20. Bias between HF radar surface currents computed with MARS and those from Garchine.

Except on edges and between islands where the reliability of radar data is questionable, the average systematic errors over time computed from Garchine measurements lie within -0.1 and 0.15 m/s over the whole area of comparison (Fig. 20); those from Brezellec measurements are around 0.05 m/s whatever the location in the critical areas mentioned before. It also appeared that, between Ushant and Sein Islands, the surface currents are underestimated by MARS model.

The average root mean square errors over MARS simulation are around 0.2 m/s with maxima around the islands. According to the comparison with both radars this deviation is acceptable for the model of concern. Such a deviation may come from: i) the depth of the first sigma level used to make these comparisons, ii) the 2-km resolution of our MARS configuration and iii) the 6-km resolution of our meteorological forcing.

This analysis allowed us to validate the simulation by MARS of the surface currents simulated by MARS despite the limitations evidenced in the vicinity of islands, where the currents are the strongest.

-Harmonic analysis

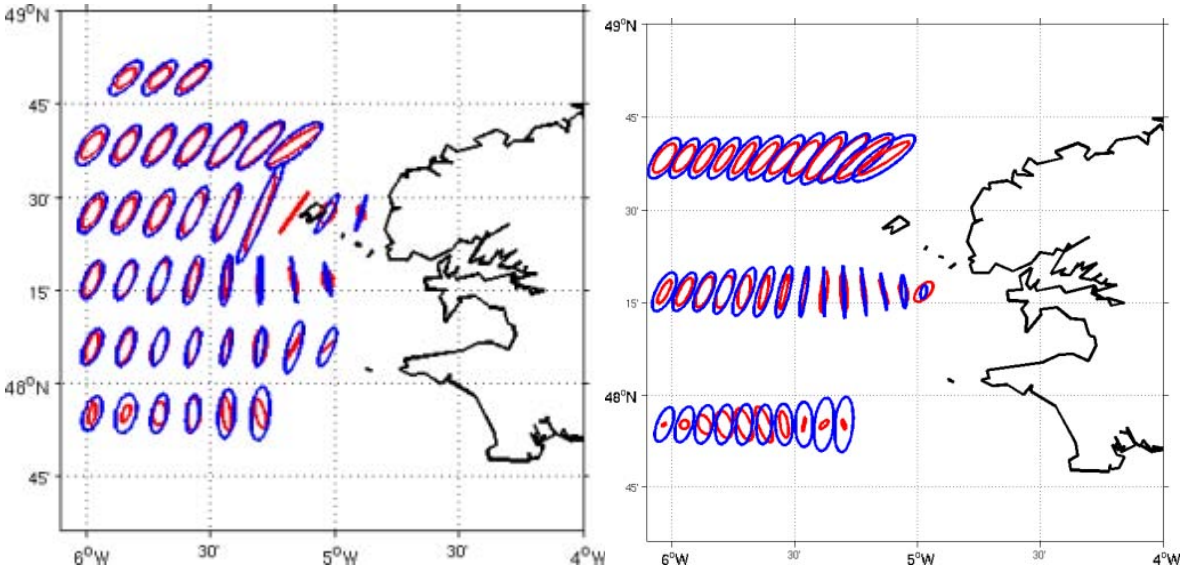

Fig. 21. Sea surface tidal current ellipses (a) for M2 and (b) for S2 from HF radar data in red and from MARS results in blue.

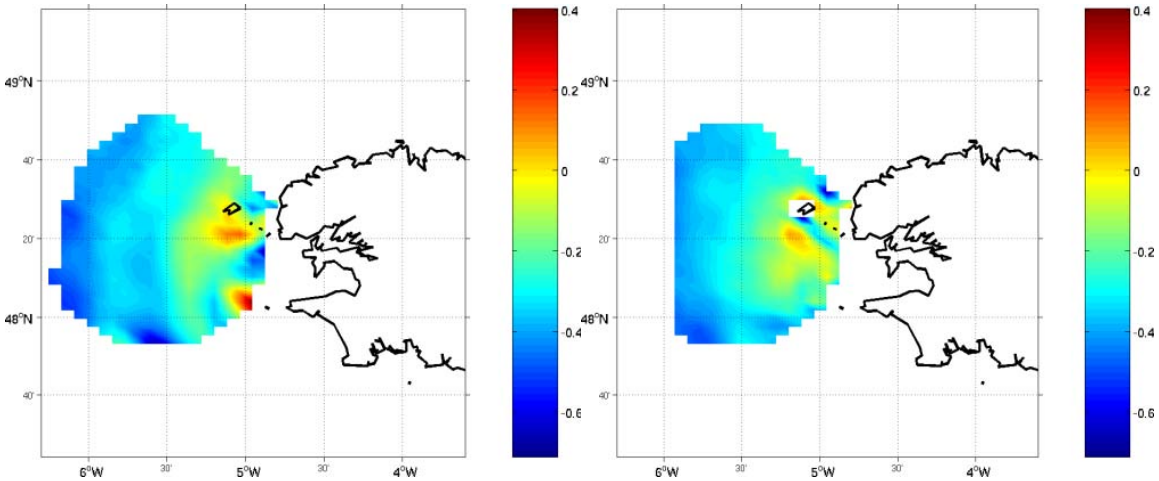

Fig. 22. Eccentricity of sea surface tidal current ellipses for M2 (a) from HF radar data (b) from MARS results.

The duration of SURLITOP experiment allowed us to conduct the harmonic analysis over 2.5 months in order to get additional information to the previous statistical analysis. According to a comparison of the sea surface tidal current ellipses for M2 and S2 from HF coastal radar observations and MARS results the tidal currents are globally in phase since they reach their maximum value at about the same time (Figs. 21a&b). The phase angle differences are the highest on the edge of measurement area. But, concerning the length of the major axis, which stands for the maximum velocity over the tidal cycle, it is overestimated by MARS almost everywhere. The mean length of the semi-major axis is 0.41 m/s for the field data, whereas it is about 0.59 m/s for the model. The deviations between field and simulation data are similar for the S2 tidal component. Thus, MARS reproduces correctly the M2 and S2 tidal components, except on the edges of the radar range. Such differences may also result from the low resolution of MARS bathymetry. In addition, as this analysis was made in Cartesian coordinates, it required to project the data located in the radar coordinate system onto a Cartesian system, which increased the error due to the radar orientation. The maps of the spatial distribution of the tidal ellipse eccentricity values (Figs. 22a & b) show that the

streams turn clockwise almost everywhere (-1 < e < 0) and that the model is globally able to reproduce it. Nevertheless, there are some isolated areas (around Ushant and Sein Islands), where the streams turn anticlockwise. MARS is unable to reproduce the area of positive eccentricity off Sein Island. One should note that when ellipses are quasi rectilinear, a difference of signs for eccentricity between the field- and simulation-data is not indicative of important bias by the model.

Given the length of the time series used to carry out this harmonic analysis, it gave very satisfactory results.

According to this first series of comparisons, MARS can accurately reproduce the instantaneous circulation in the Iroise Sea, which lets us expect that the model can deal with the temperature structure of the area.

Vertical temperature structure

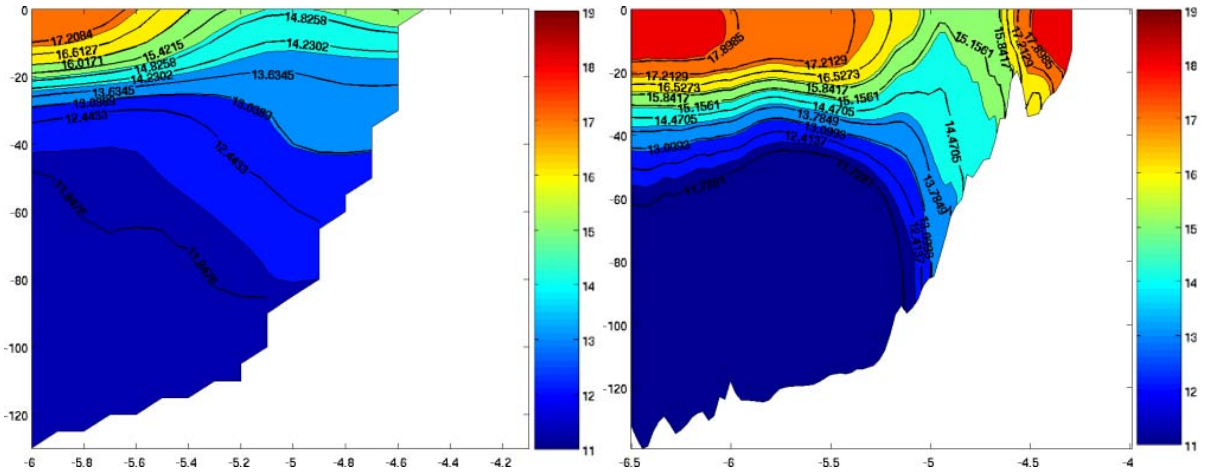

Fig. 23. Mean vertical temperature structure in July along a section located at 48.1°N for (a) the Bay of Biscay climatology and (b) MARS results.

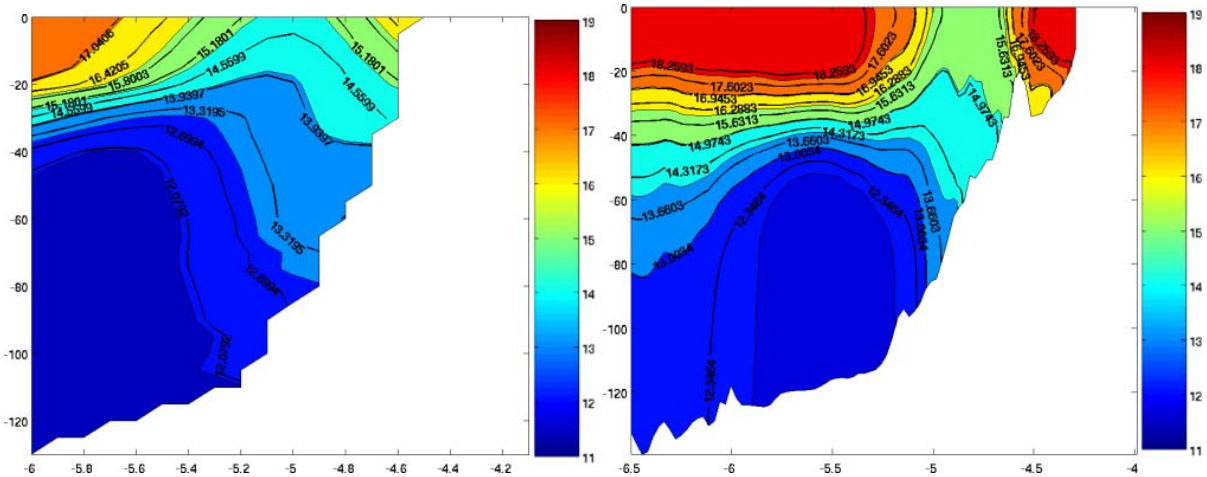

Fig. 24. Mean vertical temperature structure in August along a section located at 48.1°N for (a) the Bay of Biscay climatology and (b) MARS results.

The climatology and the monthly-averaged MARS results were compared over a period extending from early July to the end of September and on two sections: the former was located at 48.1°N and passed across the bay of Douarnenez, whereas the latter was at 48.8°N. It showed a clear reproduction by MARS of frontal structures located in the close vicinity of their true position, especially for the northern section (Figs. 23a&b). Concerning the southern section, according to the model the Ushant front is located at -5.3°W instead of -5.4°W in the climatology. In July, the internal front is poorly visible in the climatology, but it appears more clearly in August and September (Figs. 23a, 24a). The positions of the internal front in the climatology and in the averaged MARS results are in agreement in August and September. Concerning the MARS-simulated temperatures, they are globally higher than those extracted from the climatology. The difference in surface temperatures can exceed 1°C in stratified areas and reach 0.5°C in the homogeneous area (Figs. 24a&b). Incidentally, one should note that the averaged MARS temperature found in July agrees more with the climatologic situation met in August than with July one; but, as 2005 was the 12th warmer year since 1950, it may explain this overestimation trend exhibited by MARS (see part 2.1.1).
This analysis of the thermal vertical structure over July, August and September shows that the depth of the thermocline is lower of about 5 m in the model results than in the climatology (Figs. 24a&b). It may result from the meteorological forcing applied to the period under study or from an insufficient calibration of the vertical turbulent closure scheme used. Moreover, isotherms are steeper in the model outputs than in the climatology (Figs. 23a &b) because of the front oscillations with not only the spring/neap tide cycle, but also the wind gusts, at the origin of a loss of sharpness for thermal fronts in the climatology obtained from averages over more than a hundred years.

In conclusion to this analysis, the results relative to the vertical thermal structure and given by our MARS configuration are acceptable.

Sea surface temperature

-Satellite data

In order to compare the sea surface temperatures simulated by MARS and those estimated by satellites, we calculated the systematic errors, root mean square errors and standard deviations over the whole simulation and area under study. But, the reliability of the different indexes is strongly dependent on the points of comparison. In summer, satellite data are less numerous above the homogenous area, maybe because of the algorithm used for the cloud detection within the satellite data processing. On the other hand, satellite data are three times more numerous in the South West of the Bay of Audierne and off Penmarc'h headland. On average, around 20 000 points of comparison are available for the period and area of concern here.

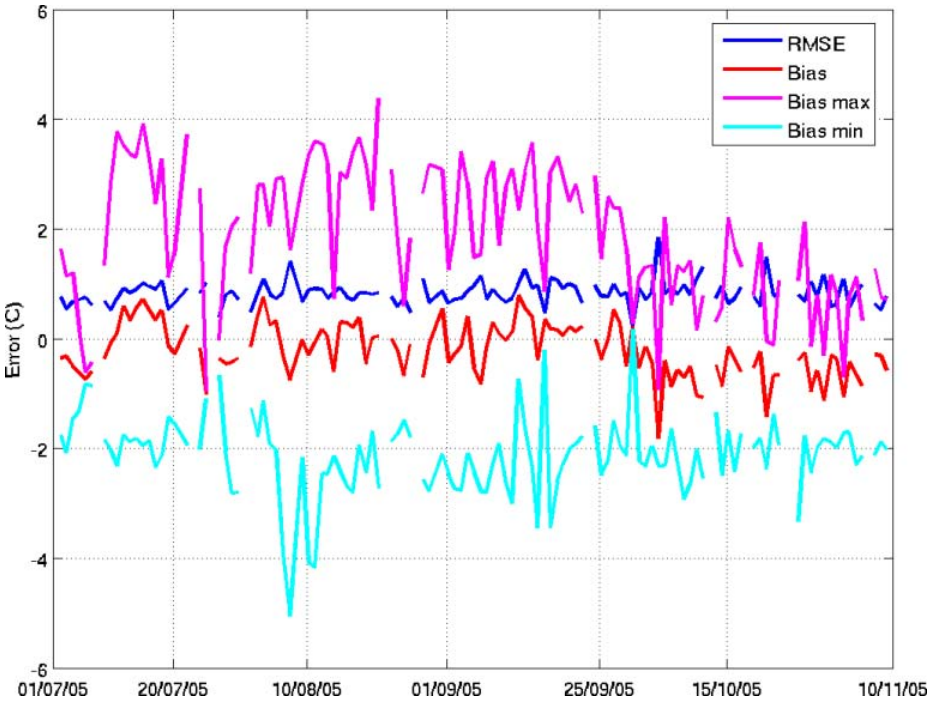

Fig. 25 Temporal evolution of Root Mean Square error, bias, maximum and minimum bias between MARS sea surface temperature and satellite data for the period from July 1 to mid-November 2005.

The calculation of the mean systematic error showed fluctuations between -0.5°C and 0.5°C, with a maximum root mean square error of about 1°C (Fig. 25). Bias and RMSE started to increase in October to, respectively, becomes close to –1°C and sometimes exceeds 1.5°C. The standard deviation of the error stays below 1°C with a slight decrease down to 0.5°C from September. During the summer, the highest and lowest systematic errors can be close to 3°C in absolute value, whereas in autumn they are nearly 2°C; this difference may come from a miscalculation of the thermal front location by MARS model.
On average, in autumn, the sea surface temperature simulated by MARS was found to be higher than the satellite measurements whereas, in summer, the model produced several spot underestimations (the highest point is about 0.5°C).

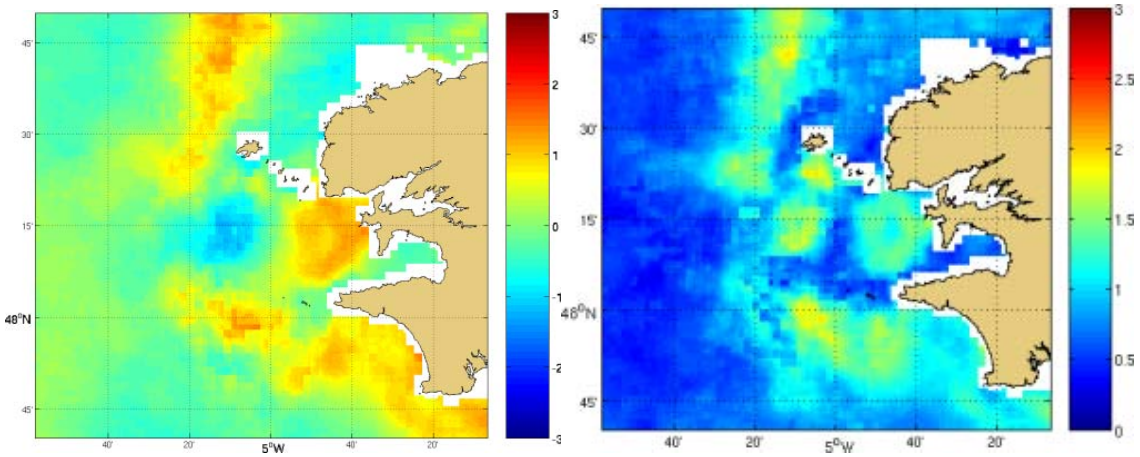

Fig. 26. Spatial repartition of (a) bias and (b) root mean square for the comparison between MARS sea surface temperature and satellite data for the period from July 1 to mid-November, 2005.

The mean systematic error and root mean square error over time both show spatial disparities (Fig 26a &b). Systematic errors are the highest at the North West of Ushant, at the

South West of Sein Island, off Crozon headland, in the bay of Audierne and off Penmarch headland (see map 1). The reason for such deviations is that, on average, the MARS-simulated Ushant front is too far from the coast whereas the internal front is too close to the coast; this arises from an overestimation of the vertical mixing on that area. Besides, the homogenous area can be divided into two homogenous areas around Ushant and Sein Islands over neap tides (see part 1); as MARS model produces no clear simulation of these phenomena, it leads to the obvious bias observed off Crozon headland and, maybe, due to either the low resolution of the bathymetry or to a limitation of the turbulent mixing scheme used.

As far as Penmarc'h and the bay of Audierne are concerned, the difference of temperatures between the model results and the field data may come from the use, in our 6-km atmospheric forcing configuration, of a land/sea mask coarser than the one used in MARS model. It may generate a bias in some wind directions taken into account by MARS as well as an overestimation of westerlies and, thus, of the upwelling effect along the coast of Penmarc'h.

It is worth noting that these spot spatial disparities are less visible in Autumn; biases are, indeed, more spatially homogeneous. Since, thermal structure are quasi non-existent at that time, these deviations may find their origin in the turbulent mixing parameterisation and in some underestimation of the surface friction by wind (see part 2.2.2). Concerning the turbulent mixing, the roughness length is assumed by the model as being constant, which induces a wrong assessment of the bottom friction.

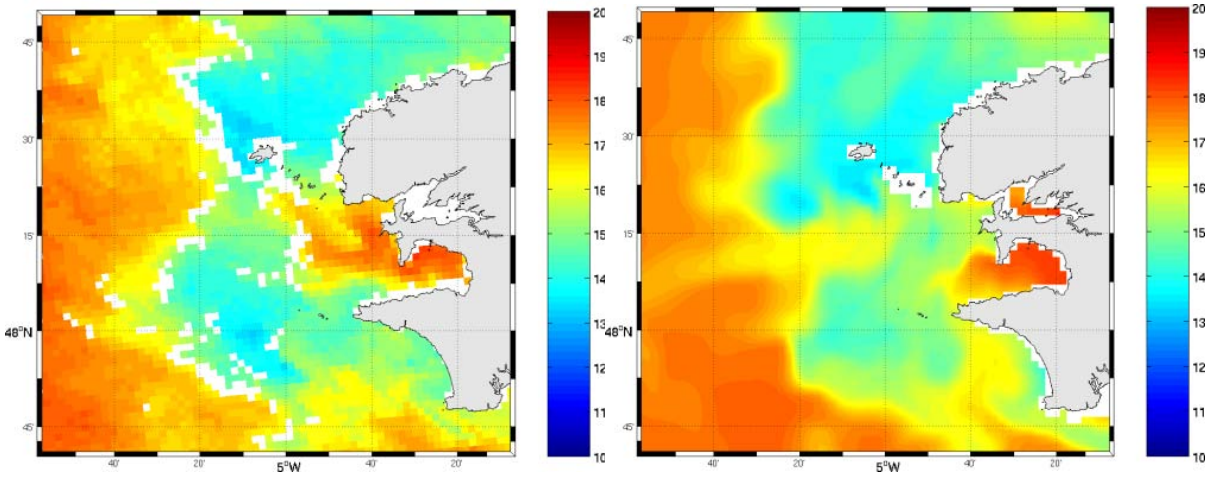

Fig. 27 Sea surface temperature (a) from satellite data, July 12, 2005 2H UTC and (b) computed with MARS, July 12, 2005 3H UTC (neap tide conditions).

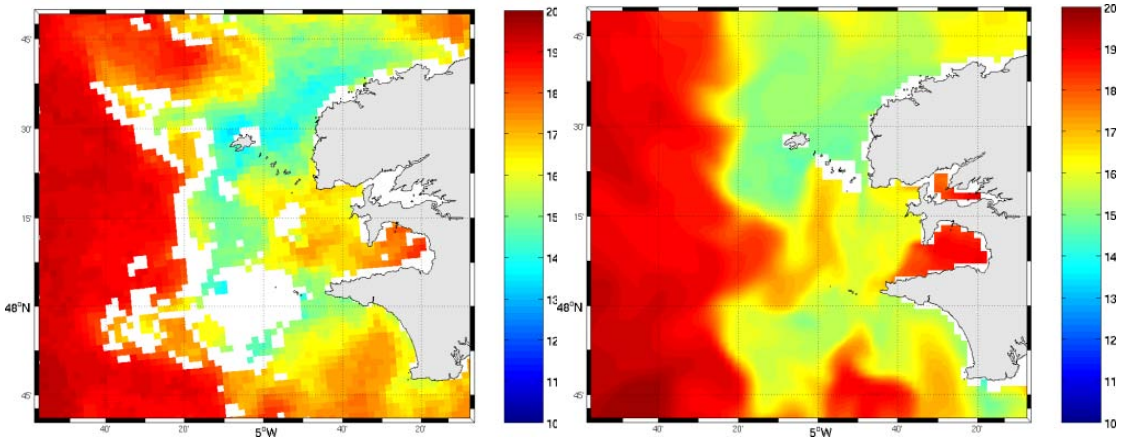

Fig. 28. Sea surface temperature (a) from satellite data, August 15, 2005 20H UTC and (b) computed with MARS, August 15, 2005 21H UTC (neap tide conditions).

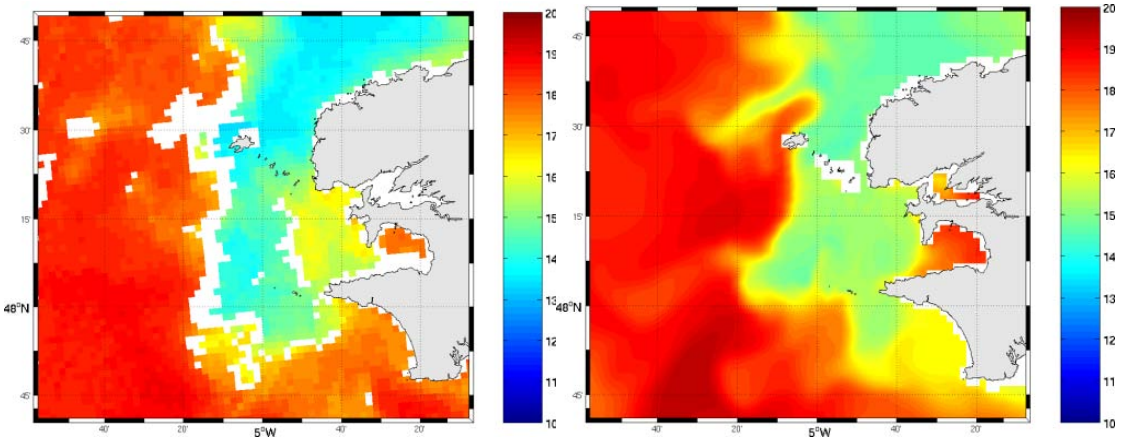

Fig. 29 Sea surface temperature (a) from satellite data, September 06, 2005 20H UTC and (b) computed with MARS, September 6, 2005 21H UTC (spring tide conditions).

The comparison of the snapshots of the sea surface temperatures issued from a satellite map (Fig. 27a) and from MARS 2-km configuration (Fig. 27b) in July shows that MARS reproduces the temporary stratified area between the islands, sometimes observed over neap tides. On the other hand, it still underestimates the sea surface temperature there. Once again, the difficulties met by MARS model to precisely locate the Ushant- and internal-fronts are highlighted by this comparison. Nevertheless, the temperatures are nearly in the same order of magnitude. In August, an obvious restratification along the North-East Finisterian coast and in the bay of Audierne visible on the satellite map appears less clearly in MARS results (Figs. 28a&b). The situation observed in September (Fig. 29a) is indicative of the trend of the homogeneous area to be closer to the coast, which is clearly reproduced by MARS (Fig. 29b). The results discussed hereabove confirm the ability of MARS to correctly reproduce the thermal structures of the Iroise Sea and their time evolution.

-"Pride of Bilbao" ferry

At this stage, it sounded worth complementing this analysis based on satellite data with sea surface temperature measurements recorded in 2005 by a ferry, the "Pride of Bilbao", which crosses the Iroise Sea almost every day to link Portsmouth (UK) to Bilbao (Spain). Its trajectories over the Iroise Sea are, first, close to -5°20' W, and then they veer to Portsmouth from Ushant.

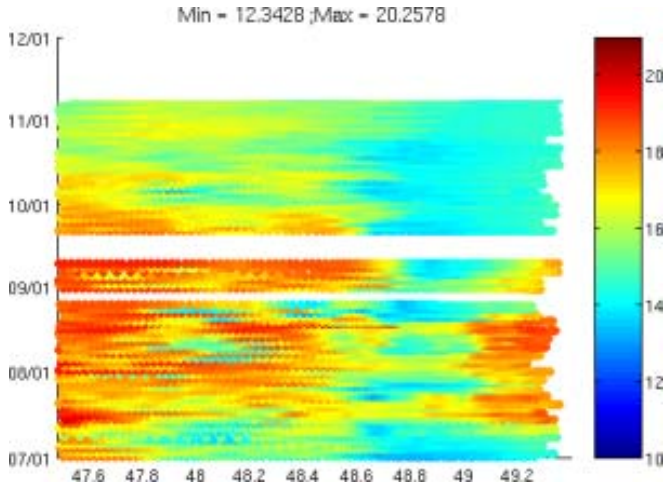

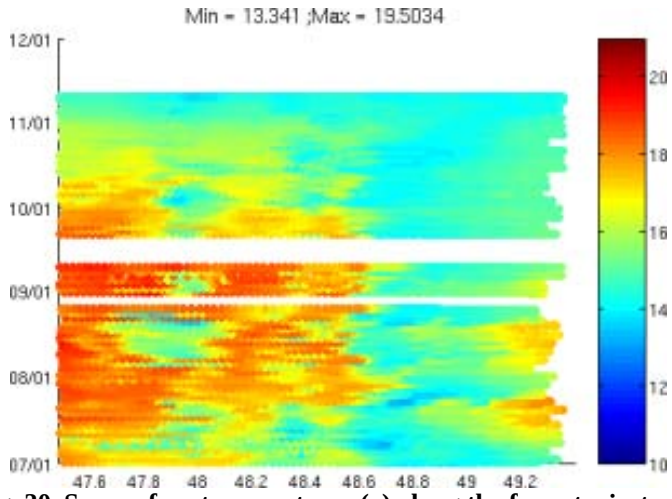

Fig. 30. Sea surface temperatures (a) along the ferry trajectories (from http://www.noc.soton.ac.uk/ops/ferrybox-2005/ferrybox_index_2005.php) (b) computed with MARS along the ferry trajectories

Figure 30a shows the sea surface temperatures taken from the dataset available for year 2005 and corresponding to every crossing between 47.5°N and 50.1°C by the ferry from July 1 to mid-November, 2005. Their comparison with the sea surface temperatures estimated by MARS along the same paths (Figs. 30a &b) underlines an underestimation by MARS in stratified area up to 48.6°N and beyond 49°N, where deviation can reach 1°C in summer. On the other hand, in the homogenous area, between 48.6°N and 49°N, the trend is an overestimation of about 0.5°C, especially from September. Nevertheless, the thermal structures are correctly represented since the sailing of the ship across successive stratified and homogenous areas is quite visible in the MARS-computed fictitious trajectories. Besides, seasonal variations in the sea surface temperature are well-reproduced by MARS.
Further to these studies, it appears that MARS can reproduce seasonal thermal fronts in the Iroise Sea, albeit with small shiftings offshore for the Ushant front and to the coast for the internal front. Moreover, the evidenced biases remain acceptable for a hydrodynamic model and MARS can be used to carry out our sensitivity study.

It is worth recalling that the simulated sea surface temperature is strongly dependent on the meteorological parameters prescribed at the air/sea interface and therefore to the climatologic sea surface temperature used for WRF boundary conditions.
This non-exhaustive analysis of comparisons between the model results and ground data allowed us to validate the tools used in this study and to be certain of the accurate reproduction of the physical processes governing the dynamics and thermodynamics in the Iroise Sea.

3.2.2 Importance of the accuracy of the meteorological forcing in ocean modelling

Impact on sea surface temperature

The four different meteorological forcings used in this study to compute the hydrodynamics and thermodynamics with MARS are:

- Hourly atmospheric forcing with a 6-km resolution computed with WRF by taking into account the sea surface temperatures of the Iroise Sea with a 10-day climatology and a 9-km spatial resolution (see part 2). (RUN 1)

- Hourly atmospheric forcing with a 18-km resolution computed with WRF by taking into account the sea surface temperatures of the Iroise Sea with a 10-day climatology and a 9-km spatial resolution (see part 2). (RUN 2)
- Hourly atmospheric forcing with a 6-km resolution computed with WRF by taking into account the sea surface temperatures of the Iroise Sea with a 10-day climatology spatially averaged over the area under study (see part 2). (RUN 3)
- Hourly atmospheric forcing with a 6-km resolution computed with WRF by taking into account the sea surface temperatures of the Iroise Sea with a daily satellite data spatially averaged over the area under study (see part 2). (RUN 4)

Hourly WRF forcings	Resolution		Sea Surface Temperature		
	6 km	18 km	10-day, 9 km	10-day, spatially uniform	1-day, spatially uniform
Run1	■		■		
Run2		■	■		
Run3	■			■	
Run4	■				■

Table 1: Summary of the different WRF forcings used in MARS simulations

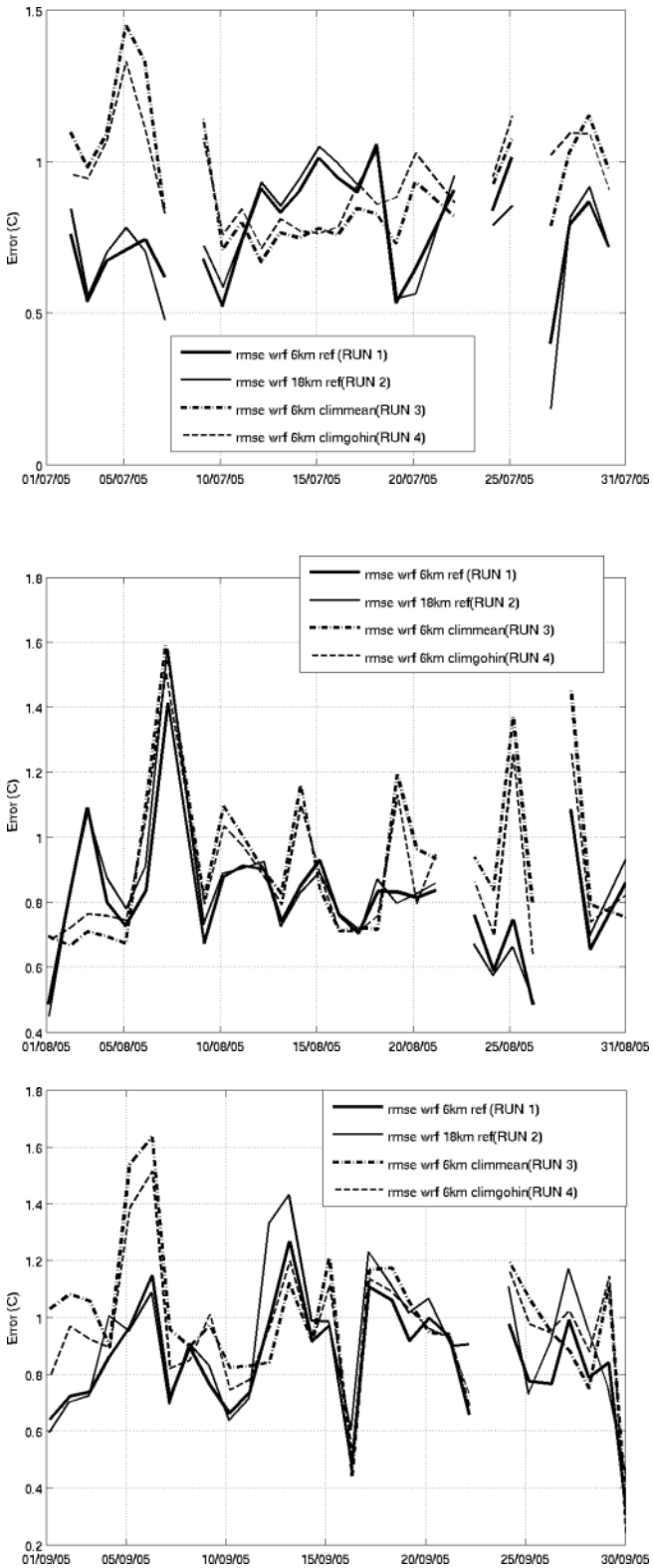

Fig. 31. Root mean square error between MARS-simulated sea surface temperatures and those from satellite data on (a) July, (b) August and (c) September.

In order to evaluate their impact on the modelling results, Figs. 31a,b&c illustrate the mean biases and root mean square errors on the sea surface temperatures (over the whole area under study) between the satellite data and those from MARS. They deal with the period covering July, August and September.

The comparison of RUN1 and RUN2 shows biases and root mean square errors over the whole area with very close temporal evolutions (Figs. 31a,b&c). In both experiments, the computed sea surface temperature is globally overestimated against satellite data. The mean deviation is about -0.1°C for RUN1 against about -0.05°C for RUN2. In addition, the mean RMSE is 0.83°C for RUN1 and is 0.86°C for RUN2. The difference between RUN1 and RUN2 is more marked in September than in July and August; for example, on September 12, 2005 there is about 0.5°C between the deviation of the numerical experiments against observations. RUN1 seems, thus, to be slightly better than RUN2.
The results produced by RUN3 and RUN4 are both clearly less satisfactory than the previous ones; on the other hand, they are quite alike (Figs. 31a,b&c) with average deviations of -0.6°C and -0.5°C, and mean RMSEs of 1°C and 0.97°C for RUN3 and RUN4, respectively.
Concerning the oceanic response, the spatial variability of the sea surface temperature used to compute meteorological forcing is, therefore, more important than its daily or nearly daily variability. Nevertheless, Fig. 31a indicates that deviation and RMSE are sometimes better in RUN3 and RUN4 than in RUN1 and RUN2, e.g. around July 15, 2005 likely because of he initial deviation between the climatology used for sea surface temperature and the true SST.

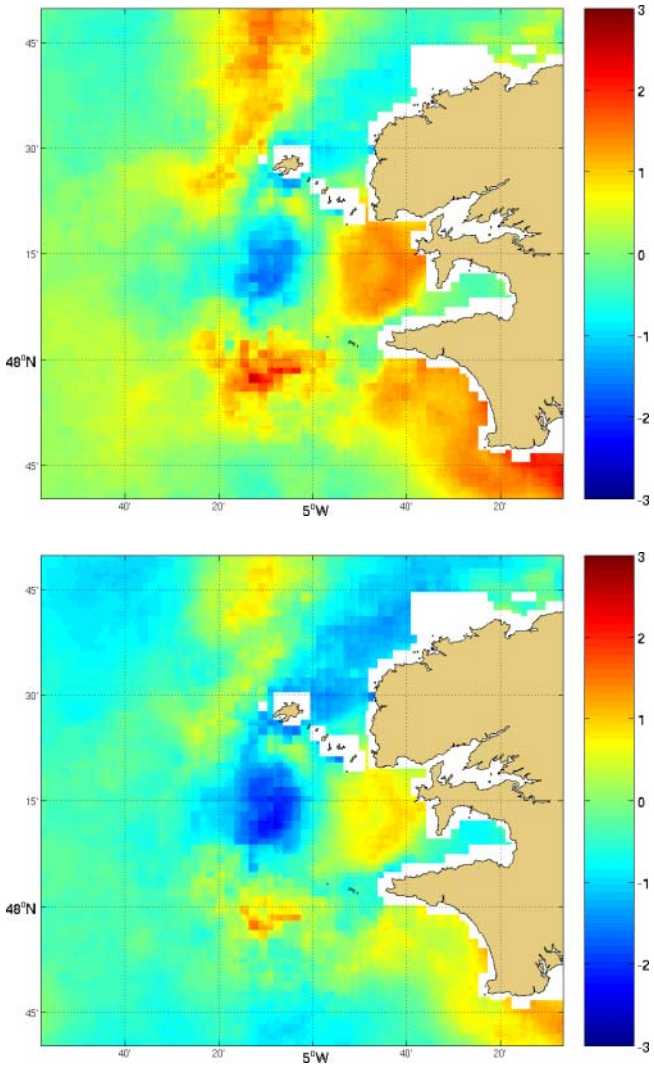

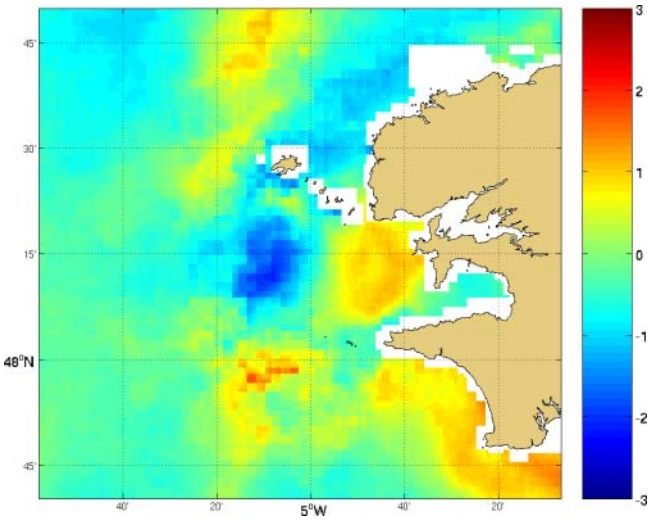

Fig. 32. Spatial distribution of bias from the comparison of MARS-produced sea surface temperatures against satellite data from July 1 to mid-November 2005 for (a) RUN2, (b) RUN3 and (c) RUN4.

To gain more insight into the relevance of atmospheric forcing-resolution and -quality, we draw the maps of time-averaged biases and RMSE over the Iroise Sea (Figs. 32a,b&c). A comparison of Figs. 26a and 32a highlights similarities in the patterns of deviation and RMSE fields in RUN2 and RUN1, except for the order of magnitude, which is higher in RUN2. Concerning RUN2, it leads to a more marked misplacement of the Ushant front off Sein Island and to a higher deviation towards data near the internal front in the bay of Audierne and near Penmarc'h. It, thus, demonstrates that the quality of the oceanic modelling near the coast and also over frontal areas is enhanced by improving the resolution of the meteorological forcing. The study of the time-averaged deviations and root mean square errors for RUN3 and RUN4 leads to less obvious conclusions than the study of their spatially-averaged statistics (Figs. 32b&c). The use of a spatial uniform SST for the computation of the meteorological parameters needed by the MARS model to calculate the heat fluxes from the Bulk formulae results in a better reproduction of sea surface temperature in frontal areas and to an overestimation in homogeneous areas as well as in offshore stratified ones. Moreover, deviations are reduced in RUN3 and RUN4 in the bay of Audierne. These differences between RUN3 and RUN4 indicate that the temporal variability of sea surface temperatures and its accuracy are a key-parameter in meteorological forcing computation studies. Indeed, the sea surface temperature is lower in the climatology near Audierne than in the reality with regards to its averaged value over the whole area; this finding explains why deviations are reduced in RUN4 at that precise location.

Thus the simulation with WRF forcing and sea surface temperature update, denoted here RUN1, presents the smallest deviation and root mean square errors compared to the reality. This was expected since the quality of meteorological parameters is directly linked to the sea surface temperature introduced in WRF.

Thus, the estimation of sea surface temperatures is enhanced by taking into account the atmospheric coastal phenomena in the regional ocean modelling. Moreover, getting accurate sea surface temperature data is paramount in modelling of regional atmospheric conditions modelling; it is, thus, essential to perform the air/sea coupling.

Impact on surface currents

The sea surface temperature and thermal structures were, thus, clearly affected by the previous forcings; however, as far as hydrodynamics is concerned, it is worth wondering whether the impact is that obvious. The comparison between the HF radar-measured surface currents and those estimated by MARS with different meteorological forcings (RUN1, RUN2, RUN3 and RUN4) gives some clues about the relevance of using WRF forcing. Indeed, the biases between measured and computed surface currents were estimated over the surface covered by HF radar from August to mid-November. The mean bias between the ground data and results from RUN1 and RUN2 and the mean correlation coefficient are around 0.03 m/s and 0.87, respectively. For such an area away from the coast, assessing the respective impacts of the 6-km atmospheric forcings and 18-km ones remains difficult. Indeed, the improvement of the surface hydrodynamics induced by a better resolution in the meteorological forcing would be noticeable near the coast, but the missing measurements prevent one from verifying it. For RUN4, the mean correlation coefficients between HF radar measurements and model results are, respectively, 0.85 and 0.87 for RUN3 and RUN4, and RUN3 and RUN4 both give a mean bias of about 0.05 m/s for the mean deviation. Even though such differences are acceptable in ocean modelling, the impact of the four different meteorological forcings upon on hydrodynamics remains still unclear. At this stage, it is worth mentioning that the use of a meteorological forcing with a 2-km resolution to take into account the climatologic sea surface temperature described in this paper cuts by ten the deviations between measurements and model results.

This discussion proves not only the importance of taking into account sea surface temperatures as realistic as possible to clearly reproduce the local coastal meteorological effects, but also that these small-scale phenomena affect the dynamics and thermodynamics of the Iroise Sea.

4 Conclusion

Because of seasonal thermal structures, the modelling of the Iroise Sea in summer is complex. These thermal fronts are at the origin of density-driven currents, which interact with the strong tidal forcing and the currents induced by variable meteorological forcing. Recent studies have evidenced the limitations of ocean modelling in accurate reproductions of the exact position of thermal fronts because of sensitivity to the applied atmospheric forcing. They led us to propose, here, the use of a high-resolution meteorological model to force a high-resolution ocean model. In order our simulations of hydrodynamics and thermodynamics within the Iroise Sea be as realistic as possible, we took into account a climatologic sea surface temperature for WRF boundary conditions and increased the space resolution with a reasonable computation time to compute the atmospheric fluxes. The use of WRF under these conditions highlighted small-scale features in wind fields like a slow-down in wind over the homogenous area of the Iroise Sea and a strong correlation between SST meso-scale patterns and relative humidity and air temperature. Even though the assessment and validation of the impacts of these very local phenomena upon on the Iroise Sea are difficult because of the lack of ground data, these investigations made appear global differences about the sea surface temperature, thermal structures and surface currents between low- and high-resolution

meteorological forcings. High-resolution forcing gave the oceanic results the closest to the reality.

Nevertheless, the meteorological parameters computed by WRF still need improvement; it can be done not only by updating WRF with sea surface temperature data of better quality, but also by increasing the resolution of WRF results to 2 km. According to experiments in progress, a third nest with a 2-km resolution in the 2-grid WRF configuration (18-6 km) can reproduce the sea/land breeze cycle as well as the wind field-acceleration along the coast and -slowdown in the lee of obstacles such as Ushant island. Moreover, despite the low altitude of Brittany, the wind field is affected by the uneven coastline. The difference between the 2-km WRF results and the 6-km ones is low for the winds measured far from the coast. On the other hand, near the coast, the 2-km configuration reveals local coastal phenomena unsuspected in the low-resolution meteorological forcing available today for such an ocean modelling.
Concerning the enhancement of the sea surface temperature employed in WRF, the use of an air/sea coupling would lead to a better consistency between the exchanges at the air/sea interface. Moreover, it would certainly affect the thermal structure position. Besides, the introduction, in this coupled system, of roughness parameter, which is linked to the sea state and to the surface currents, would induce an impact by tides upon the meteorological field; for weak winds, it would also consider the currents driving effect created when the water mass drags air from the low atmospheric layers..

About the relevance of high-resolution forcing for a regional ocean modelling, our MARS simulations revealed interesting oceanic features whose evolution would be worth being studied in relation with the atmospheric forcing applied to the sea surface.

Acknowledgements: We acknowledge the ACTIMAR company for its financial support and for setting at our disposal high-frequency radar data collected within the framework of SURLITOP project initiated by the RITMER network. We are grateful to SHOM (the French naval hydrographic and oceanographic service) for provision of bathymetry data. The sea surface temperature data have been produced by SAF (Satellite Application Facility) of EUMETSTAT/Météo-France and provided through CERSAT Internet satellite image browser. The authors thank Francis Gohin and all of the satellite data providers for making data available to the scientific community. We also acknowledge Météo-France for providing us with data from the meteorological stations located in the Iroise Sea under the agreement between Méteo-France and the University of Western Brittany (UBO). We thank also Frédéric Vandermeirsh for making us available the results issued from the monthly climatology of the Bay of Biscay.

References

Altazin-Pichon A. (1981) Application d'un modèle de thermocline à la formation du front thermique en mer d'Iroise. Confrontation des résultats avec des mesures in situ. Thèse de doctorat de spécialité (océanographie physique), Université de Bretagne Occidentale, Brest, 140pp.

Birrien J. L. (1987) Cycles de variations des éléments nutritifs et du phytoplancton en baie de Douarnenez et dans les secteurs adjacents : Importance du front côtier de l'Iroise, Thèse de doctorat, Université de Bretagne Occidentale, Brest, 160pp.

Chen, F., and J. Dudhia (2001) Coupling an advanced land-surface/hydrology model with the Penn State/ NCAR MM5 modelling system. Part I: Model description and implementation. Mon. Wea. Rev., 129, 569-585.

Cochin V. (2006) Evaluation of ground wave HF/VHF radars for operational oceanography, PhD thesis.

Davies H. C., Turner R. E. (1977) Updating prediction models by dynamical relaxation: An examination of the technique. Quart. J. Roy. Meteor. Soc., 103: 225-245.

Faugère Y., Le Borgne P., Roquet H. (2001) Réalisation d'une climatologie mondiale de la température de surface de la mer à échelle fine. Météo France, Direction de la production, Centre de Météorologie Spatiale. La Météorologie 35.

Fels, S.B. and M.D. Schwarzkopf (1975) The simplified exchange approximation: a new method for radiative transfer calculations, J. Atmos. Sci., 32, 1475-1488

Ferrier B. S., Jin Y., Lin Y., Black T., Rogers E., Dimego G. (2002): Implementation of a new grid-sc ale cloud and precipitation scheme in the NCEP Eta model. Preprints, 15th conf on Numerical Weather prediction, Amer. Meteor. Soc., San Antonio, TX, 280-283.

Gaspar P., Grégoris Y., Lefevre J. M. (1990) A simple eddy kinetic energy model for simulations of the oceanic vertical mixing: tests at station Papa and long-term upper ocean study site, J Geophys. Res., 95: 16179-16193.

Geernaert,G. L., and K. B. Katsaros, (1986) Incorporation of stratification effects on the oceanic roughness length in the derivation of the neutral drag coefficient. J. Phys. Oceanog., 16, 1580-1584.

Janjic, Z.I. (1990) The step-mountain coordinate physical package, Mon. Wea. Rev., 118, 1429-1443.

Janjic, Z.I., (1994) The step-mountain eta coordinate model: further developments of the convection, viscous sublayer and turbulence closure schemes, Mon. Wea. Rev., 122, 927-945.

Janjic, Z.I., (1996) The surface layer in the NCEP Eta Model, Eleventh Conference on Numerical Weather Prediction, Norfolk, VA, 19-23 August; Amer. Meteor. Soc., Boston, MA, 354-355.

Janjic, Z.I., (2000) Comments on « Development and Evaluation of a convertive scheme for Use in Climate Models", J. Atmos. Sci., 57, p.3686

Janjic, Z.I., (2002) Nonsingular Implementation of the Mellor-Yamada Level 2.5 Scheme in the NCEP Meso model, NCEP Office Note, No. 437, 61pp.

Klemp J., Skamarock W. C., Dudhia J (2000) Conservative split-explicit time integration methods for the compressible nonhydrostatic equations: WRF Eulerian prototype model equation on height and mass coordinates.

Lacis, A. A., and J.E. Hansen (1974) A parameterization for the absorption of solar radiation in the earth's atmosphere. J. Atmos. Sci., 31, 118-133.

Lazure P., Dumas F. (accepted) A 3D hydrodynamics model for applications at the regional scale (MARS-3D): application to the bay of Biscay. Advances in water resources.

Le Cann B. (1982) Evolution annuelle de la structure hydrologique du plateau continental au Sud de la Bretagne. Modélisation numérique. Thèse de doctorat de 3ème cycle en Océanographie Physique. Université de Bretagne Occidentale BREST, 251pp.

Le Duff M., Hily C. (1999) Environnement Naturel de l'Iroise. Bilan des connaissances et Intérêt patrimonial. Etude réalisée dans le cadre d'une convention DIREN Bretagne et l'Université de Bretagne Occidentale Volume 2, 83pp.

Le Fèvre J., Grall J. R. (1970) On the relationships of Noctiluca swarming off the western coast of Brittany with hydrological feature and plankton characteristics of the environment. Journal of Experimental Marine Biology and Ecology, 4:287:306.

Lefèvre F., Lyard F. H., Le Provost C., Schrama E. J. O. (2002) FES99: A global Tide Finite Element Solution Assimilating Tide Gauge and Altimetric Information. Journal of Atmospheric and Oceanic Technology: Vol. 19, No.9: 1345-1356.

Luyten P., De Mulder T. (1992) A module representating surface fluxes of momentum and heat, MUMM's technical report#9, 30pp.

Mariette V. (1983) Effet des échanges atmosphériques sur la structure thermique marine. Application à des zones du large et à une zone côtière, Thèse de doctorat ès Sciences Physiques, Université de Bretagne Occidentale, Brest, 282pp.

Mariette V., Le Saos J. P., Rougier G. (1983) Résultats des mesures d'océanographie physique réalisées lors de la campagne Satir-Dynatlant. Rapport Scient., Lab. Océano. Phys., Université de Bretagne Occidentale, Brest, 110pp.

Mariette V., Rougier G., Salomon J. C., Simon B. (1982) Courants de marée en Mer d'Iroise. Oceanologica Acta. 5, 2:149-159.

Mariette V., Le Corre P. (1982) Le front thermique d'Ouessant en août et septembre 1982, campagne Satir Dynatlant. Campagne océanographique française N°1-1985. IFREMER, 369pp.
Mariette V., Le Cann B. (1985) Simulation of the formation of Ushant thermal front. Cont. Shelf Res. 4 (6), 637-660

Morin P. (1984) Evolution des éléments nutritifs dans les systèmes frontaux de l'Iroise : assimilation et régénération ; relation avec les structures hydrologiques et les cycles de développement du phytoplancton, Thèse de Doctorat, Université De Bretagne Occidentale, Brest, 220pp.

Pingree R. D., Holligan P. M., Head R. N. (1977) Survival of dinoflagellate blooms in the western English Channel, Nature, 265, 266.

Schwarzkopf, M.D. and S.B. Fels (1991) The simplified exchange method revisited – An accurate, rapid method for computation of infrared cooling rates and fluxes. J. Geophys. Res., 96 (D5), 9075-9096.

Skamarock W. C., Time splitting techniques for multidimensional transport, available at http://www.mmm.ucar.edu/individual/skamarock/advect3d_2005.pdf, 26pp.

Smagorinsky J. (1963) General circulation experiments with the primitive equation. I. The basic experiment. Monthly Weather Review 111:99-165.

Wicker L. J., Skamarock W. C. (2002) Time splitting methods for elastic models using forward time schemes, Mon. Wea. Rev., 130: 2088:2097

Young E. F., Brown J., Aldridge J. N. , Horsburgh K. J., Fernand L. (2004) Development and application of three-dimensional baroclinic model to the study of the seasonal circulation in the Celtic Sea, Continental Shelf research, 24:13-36.

Static data for WRF: ftp://aftp.fsl.noaa.gov/divisions/frd-laps/WRFSI/Geog_Data

Figure legends